Dynamics of H_2O_2 photodissociation: OH product state and momentum distribution characterized by sub-Doppler and polarization spectroscopy

Karl-Heinz Gericke, Stefan Klee, and Franz Josef Comes
Institut für Physikalische und Theoretische Chemie der Johann Wolfgang Goethe-Universität, Niederurseler Hang, 6000 Frankfurt am Main 50, Federal Republic of Germany

Richard N. Dixon
School of Chemistry, University of Bristol, Cantock's Close, Bristol BS8 1TS, United Kingdom

(Received 3 June 1986; accepted 11 July 1986)

Hydrogen peroxide has been optically excited at a wavelength of 266 nm and the OH photofragment completely characterized by Doppler and polarization spectroscopy using the laser-induced fluorescence technique. The entire internal state distribution (vibration, rotation, spin, and Λ components), translational energy, angular distribution, rotational alignment, and vector correlations between rotational and translation motions of OH products is measured. The hydroxyl radicals are formed in the $X\,^2\Pi_{3/2,1/2}$ ground state with 90% of the available energy (248 kJ/mol) being released as OH recoil translation. The angular distribution is nearly a $\sin^2\theta$ distribution about the electric vector of the photolysis laser. The internal motion of OH is vibrationally cold (no vibrationally excited OH was found) while the rotational excitation in $v'' = 0$ can be described by a Boltzmann distribution with a temperature parameter of $T_{\rm rot} = (1530 \pm 150)$ K. The two spin states are found to be populated nearly statistically, in contrast to the Λ components which show an increasing inversion with increasing OH rotation. The observed profiles of recoil Doppler broadened spectral lines are strongly dependent on the nature of the transition, the excitation–detection geometry, and the relative polarizations of the dissociating and analyzing laser light. However, the line intensities show only a minor dependence on geometry and polarization indicating a low alignment of OH photofragments ($A_0^{(2)} \leqslant 0.1$). For the first time the vector correlation between product rotational and translational motions was analyzed and evaluated in terms of the three bipolar moments $\beta_0^2(20)$, $\beta_0^0(22)$, and $\beta_0^2(22)$. The bipolar moment $\beta_0^2(20)$ corresponds to the conventionally defined anisotropy parameter $\beta = 2\beta_0^2(20) = -0.71$. The angular distribution peaks in the direction perpendicular to the electric vector of the dissociating laser light, indicating the predominant electronic excited state in H_2O_2 being of ^1A symmetry. The moment $\beta_0^0(22)$ increases with $J_{\rm OH}$ showing a bias towards $\mathbf{v}_{\rm OH}$ and $\mathbf{J}_{\rm OH}$ being parallel to one another. The moment $\beta_0^2(22)$ is a measure of the mutual correlation of the fragment translational and rotational vectors and the transition dipole vector $\boldsymbol{\mu}$ in the parent molecule. The positive value of this moment $[\beta_0^2(22) = 0.11]$ indicates that the expectation value of $\langle J_y^2 \rangle$ should be very small when $\boldsymbol{\mu}$ is parallel to the z axis and $\mathbf{v}_{\rm OH}$ perpendicular to $\boldsymbol{\mu}$ (x axis). $\langle J_x^2 \rangle$ originates in the torsional motion in the H_2O_2 parent molecule, while $\langle J_z^2 \rangle$ reflects the bending vibration of nearly planar H_2O_2 where the H atoms are in the *trans* position.

I. INTRODUCTION

The fascinating aspect of photodissociation dynamics is the possibility of studying a primary chemical event, where the molecule can be optically prepared in a relatively narrow distribution of parent excited states. The products can be analyzed in detail similar to studies concerning reaction dynamics. A complete characterization of the photodissociation dynamics involves not only the knowledge of nascent internal state distributions and translational energy of the fragments, but also the knowledge of product angular distributions, correlation of the rotational motion of the product with the alignment of the parent molecule, dependence of the photofragment rotation on its translational motion, and correlation between the transition dipole moment in the parent and the translational and rotational motions of the product.

Laser-induced fluorescence (LIF) or (resonance enhanced) multiphoton ionization are common methods to measure the internal state distribution of photofragments under collision free conditions.[1] The domain of mass spectroscopy combined with time-of-flight measurements is the analysis of product angular distributions in a molecular beam.[2–6] But the low resolution of these experiments does not permit a detailed analysis for state selected product quantum states. Recently, Doppler spectroscopy using LIF has been applied to study the velocity distribution and rotational alignment of fragments in bulk and molecular beam experiments.[7–12] Dubs *et al.* have measured the correlation between the rotational alignment and the direction of recoil of NO photoproducts in the dissociation of dimethylnitrosamine.[11] Some features of polarization Doppler spectroscopy in order to elucidate $\mathbf{v}$–$\mathbf{J}$ correlation in molecular photodissociation were presented recently by Hall *et al.*[13] The authors treat in their preliminary analysis variations of Doppler profiles in the special case of the $Q(59)$ and $P(59)$ rotational

 0021-9606/86/204463-17$02.10

transitions of CO from photodissociated OCS at 222 nm.

The single photon photolysis of H_2O_2 at 248 and 193 nm shows no generation of electronically excited OH and both fragments are formed in the $X\,^2\Pi_{3/2,1/2}$ ground state. The available energy is mostly transferred into fragment recoil[14] and only a small part can be found in OH product rotation.

At excitation wavelengths below 172.2 nm electronically excited hydroxyl radicals could be identified at their characteristic OH($A\,^2\Sigma \rightarrow X\,^2\Pi$) resonant transitions.[15] Gölzenleuchter *et al.* observed that most of the released energy is transferred into OH rotation when hydrogen peroxide is excited at 157 nm.[16] It was demonstrated that in a two-photon process at 193 nm OH photofragments are also formed in the $A\,^2\Sigma$ state.[17,18]

In a previous work[19] we investigated the nascent translational and anisotropic angular distribution of recoiling OH photofragments and obtained information about lifetime and symmetry of the excited dissociative state. The angular distribution measured by Doppler spectroscopy peaks in the direction perpendicular to the electric vector of the dissociating laser light. The predominant electronic excited state (at 266 nm) in hydrogen peroxide was found to be of ^1A symmetry. The excited H_2O_2 parent molecule has a lifetime of less than 60 fs.

The present paper reports on a detailed investigation of the one photon excitation and dissociation of hydrogen peroxide at 266 nm,

$$H_2O_2(\tilde{X}\,^1A) + h\nu(\lambda = 266\text{ nm}) \rightarrow H_2O_2(\tilde{A}\,^1A) \rightarrow OH(^2\Pi) + OH(^2\Pi), \quad (1)$$

which gives OH products in the electronic ground state exclusively. Not only the entire internal state distribution could be determined, including such fine effects as Λ and spin-doubling, but also the translational motion and molecular alignment were detected. The most important aspect of this experiment, however, is related to an evaluation of the observed Doppler profiles of recoiling OH photofragments which reflects the anisotropic character of the dissociation process (1). In this paper we analyze in detail *vector* correlations between the rotational and translational motion of the OH product and the transition dipole of the H_2O_2 parent molecule. This type of study of isolated fragment states employing a polarized probe laser with sub-Doppler resolution gives a deep insight into scalar and vectorial properties of reaction processes.

II. EXPERIMENTAL

The experimental arrangement has been described previously[19] in connection with our earlier measurements of OH Doppler line shapes in the 266 nm photolysis of hydrogen peroxide. The only significant modification in the additional analysis of nascent distributions of OH fragments over the various rotational and fine structure states was the broadband operation of the probe laser. Briefly, the 266 nm photodissociating light stemmed from the frequency quadrupled output of a Nd:YAG laser (Spectron, SL2Q), that delivered 12 ns pulses of typically 12 mJ at a repetition rate of 12.5 Hz. Prior to entering slightly focused the cubic aluminum chamber through a baffled arm, the horizontally polarized photolysis beam passed through a rotatable half-wave retardation plate giving the possibility to turn the plane of the electric vector $\mathbf{E}_p$ by 90°.

The required tunable laser radiation for resonant excitation of OH was provided by a frequency doubled dye laser (Lambda Physik, FL 2002 E, Rhodamin 101 in methanol; Inrad autotracking unit), which was pumped after an optical delay of 17 ns by the second harmonic of the same Nd:YAG laser. Saturation as a fundamental source of error in LIF detection was avoided by attenuating the dye laser output to energies less than 1 μJ per pulse, which was experimentally confirmed by the linear dependence of the fluorescence signal on the probe laser energy. The analyzing beam was used unfocused but collimated by baffles to a diameter of 3 mm. For distribution measurements in the range of 306–312 nm, i.e., the R and Q branches of the (0,0) band in the OH($X\,^2\Pi \rightarrow A\,^2\Sigma^+$) transition, the dye laser was used in broadband operation (0.50 cm^{-1} FWHM). On the contrary, analysis of Doppler line shapes took place with a bandwidth narrowed laser (0.11 cm^{-1} FWHM) applying a stepping motor tuned intracavity etalon.

The dye laser was carefully adjusted to overlap with the photodissociating laser beam in the middle of the cell. Experiments were performed under both the counterpropagated coaxially probed geometry and the mutually orthogonal geometry. The latter arrangement yielded a considerably weaker fluorescence signal in comparison to the former one due to the much smaller interaction area. The eight possible configurations originating from the various beam and polarization directions are shown in Fig. 1: $\mathbf{E}_p$ is always drawn parallel to the z axis; designation as H or V means horizontal or vertical polarization of the photolysis (subscript p), respectively, analyzing laser (subscript a). A prime indicates experimentation under mutually orthogonal geometry.

LIF was viewed at right angles to the plane formed by the two beams with a photomultiplier tube (Hamamatsu, R 955; 1.2 kV) equipped with an imaging optics and an interference filter (310 $\pm$ 10 nm). The PMT voltage was measured and averaged with a PAR 162/165 boxcar integrator connected to a computer, which controlled the experiment and normalized the signal to the photolysis and probe laser energies for individual laser shots.

To guarantee for comparable experimental conditions from one photolysis shot to the other H_2O_2 (90%) was kept flowing rapidly through the cell at a pressure of typically 100 mTorr.

The detected OH absorption spectrum from dissociated H_2O_2 at 266 nm was analyzed on basis of the classic work of Dieke and Crosswhite (DC),[20] whereas the spectroscopic line assignments followed Herzberg's notation.[21] The latter notation with its generalized symbol ${}^{\Delta N}\Delta J_{F,f}$ is useful to demonstrate in cases of satellite lines, stemming from violation of the $\Delta N = 0, \pm 1$ selection rule of Hund's case (b), to which main branch in terms of the other rule $\Delta J = 0, \pm 1$ these transitions really belong. This knowledge facilitates the understanding for different behavior of main and satellite transitions of the same branch according to DC's notation as is observed in line shape measurements (*vide infra*). For example, a P_{12} satellite really belongs to the Q branch.

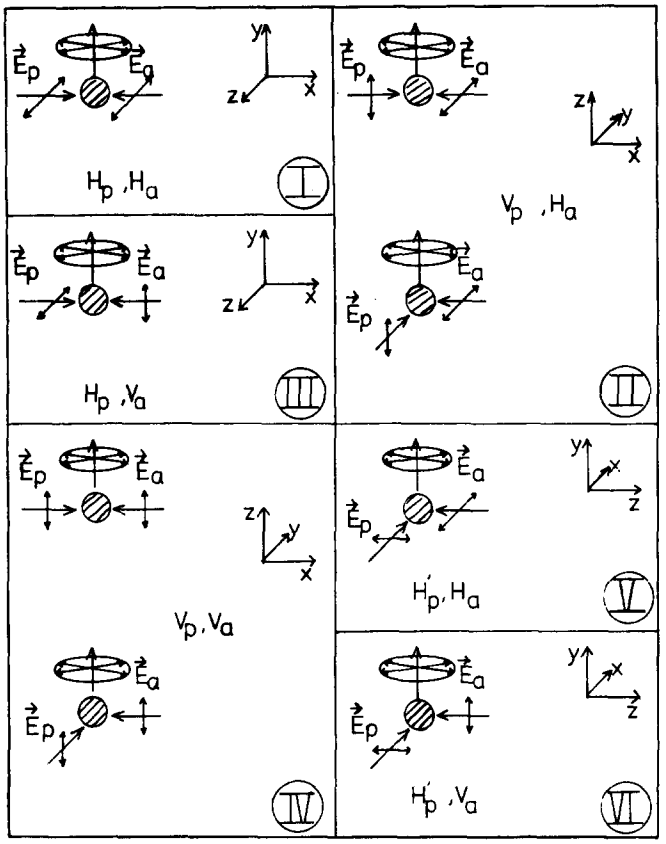

FIG. 1. Characterization of the six different photolysis–analysis detection geometries (I–VI) which were used to determine the population distribution and Doppler profiles of OH products formed by the photolysis of H_2O_2 at 266 nm. Horizontal or vertical polarization of each beam is designated as H or V; a prime indicates the mutually orthogonal geometry. The undispersed laser-induced fluorescence light was detected always perpendicular to the propagation direction of both laser beams. Detection optics and photomultiplier accepted all polarizations equally.

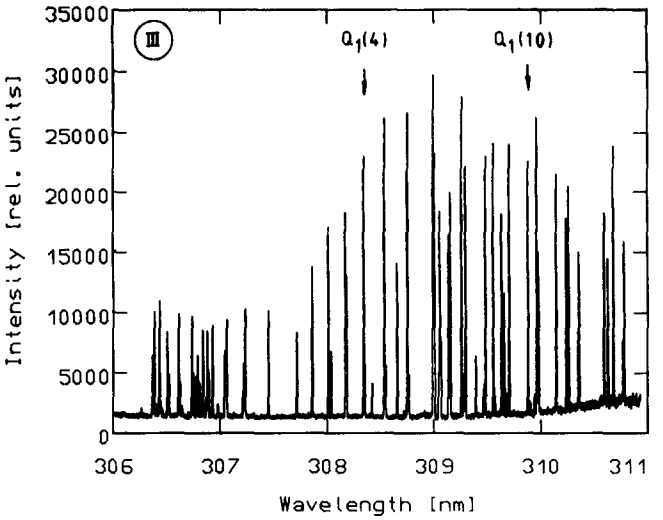

FIG. 2. Excitation spectrum of $OH(X\,^2\Pi)$ photofragments generated by the photolysis of H_2O_2 at 266 nm, the wavelength of the fourth harmonic of the Nd:YAG laser. This spectrum has been normalized with respect to the analyzing dye and the dissociating Nd:YAG laser light. Experimental conditions at geometry III (see Fig. 1) were: $P_{tot} = 100$ mTorr, 17 ns time delay between the two laser pulses.

The relations between both notations concerning OH satellite lines are as follows: $Q_{12} \Leftrightarrow {}^qR_{12}$, $Q_{21} \Leftrightarrow {}^qP_{21}$, $R_{21} \Leftrightarrow {}^rQ_{21}$, $S_{21} \Leftrightarrow {}^sR_{21}$, $P_{12} \Leftrightarrow {}^pQ_{12}$, $O_{12} \Leftrightarrow {}^oP_{12}$.

II. ALIGNMENT AND POPULATION DISTRIBUTION OF OH PHOTOPRODUCTS

The OH photofragment distribution in the $v'' = 0$ level is probed by excitation of the $X\,^2\Pi(v'' = 0) \rightarrow A\,^2\Sigma(v' = 0)$ band. Figure 2 shows a scan of this band for the OH products generated by the photolysis of H_2O_2 at 266 nm. The internal state distributions are not directly deducible from these observed line intensities. First we have to consider fluctuations in the output power of the dissociating Nd:YAG laser and the analyzing dye laser by normalizing the observed fluorescence light with respect to these pump and probe intensities. Then the OH fragments may be aligned resulting in, for example, a preferred detection of the Q branch at the expense of the P and R transitions. Thus one has to take into account the effects of J_{OH} alignment to deduce reliable product state populations.

A. OH fragment alignment

The rotational anisotropy of photoproducts can be determined by measuring the relative line intensities at different geometries and polarizations of an exciting dye laser beam.[9–11,13] Theoretical derivations have been developed which describe the correlation of the rotation with the alignment of the parent molecule transition moment.[22–27]

General expressions were obtained for the intensity I of polarized light is emitted in any direction following an arbitrary excitation process. The intensity I is expressed in terms of simple geometrical factors and dynamical parameters $(A_0^{(k)})$ corresponding to multipole expansion terms of the total angular momentum density matrix. Greene and Zare have given a general formula for the dependence of the LIF intensity on the incident and emitted light directions and polarizations for axially symmetric systems [Eq. (1) in Ref. 25].

In the case of photodissociation with linearly polarized light the density matrix has only two nonzero moments. These are the monopole moment $A_0^{(0)} = 1$ and the quadrupole moment $A_0^{(2)}$, which is $A_0^{(2)} = 0$ for $J = 0,1/2$; and lies between the limits

$$-\tfrac{2}{5} \leqslant A_0^{(2)} \leqslant +\tfrac{4}{5} \qquad (2)$$

for high J. The limiting cases of $A_0^{(2)} = -\tfrac{2}{5}$ and $A_0^{(2)} = +\tfrac{4}{5}$ correspond, respectively, to the limiting cases of fragment rotation perpendicular, and parallel, to the parent molecule transition dipole.

The alignment parameter $A_0^{(2)}$ can be obtained by evaluating the ratio of the intensities for different geometries. The Q branches are the most sensitive to a change in the experimental photolysis probe between geometries III and IV. Such an analysis would require a careful adjustment of the two laser beams because variations in the line intensities at different geometries will be interpreted as alignment of the OH photofragment. Therefore, we used an alternative procedure to determine the alignment parameter.

The $A_0^{(2)}(J)$ can be calculated forming the ratio of the intensities of main, I_m and accompanying satellite line, I_s,

originating from the same lower level. In a single geometry their relative intensities directly yield the value of $A_0^{(2)}$ and its possible J_{OH} dependence. We exclude influence of saturation by using the overall ratio of I_m/I_s (III) for geometry III to I_m/I_s (IV) for geometry IV to determine the parameter $A_0^{(2)}$ as a function of OH rotation. The values obtained are shown graphically in Fig. 3. The OH fragment shows only a slight alignment in the present photodissociation processs of H_2O_2. The largest values of $A_0^{(2)}$ were found to be 0.1; far from the limiting value of $A_0^{(2)}(\max) = \frac{4}{5}$ for J parallel to μ. At higher OH rotations ($N_{OH} > 8$) $A_0^{(2)}$ seems to decrease again. The large error bars relative to the small values of the alignment parameter—a consequence of uncertainties in small differences between large numbers—do not permit to draw very detailed conclusions from these experimental findings.

For calculating populations of the internal state distributions including the correction with regard to OH alignment the following equation was applied using the arithmetic mean of $A_0^{(2)} = 0.075$:

$$P(J) \sim I/[B(a_0 + a_1 A_0^{(2)})]. \tag{3}$$

The transition probabilities B as well as the energy levels of OH radicals were taken from the literature.[28,29] The parameters a_0 and a_1 depend on the excitation–detection geometry and the angular momentum coupling, described in Sec. IV A.

Although the OH photodissociation products exhibit only a minor correlation between angular momentum and dissociation polarization direction, the recoil velocity and rotational motion of the fragments are strongly correlated. This correlation does not alter the integrated line intensities but the shape of Doppler profiles varies strongly when different detection geometries or branches are used in probing the OH fragment. An analysis of the inter-relation of translational and rotational motions of photoproducts will be accomplished in Sec. IV.

B. OH rotational distribution

The rotational state distribution of the $v'' = 0$ vibrational level of OH was analyzed by fitted the data to a Boltzmann distribution

$$P(J) \sim (2J+1)\exp(-E_{rot}hc/kT_{rot}). \tag{4}$$

If a plot of $\ln[P(J)/(2J+1)]$ vs E_{rot} can be represented by a straight line, then the distribution is Boltzmannian and is characterized by a single parameter T_{rot}, the "rotational temperature." Such a plot is shown in Fig. 4 for both the $^2\Pi_{3/2}$ and the $^2\Pi_{1/2}$ spin system. The distribution observed can obviously be described by a straight line with a rotational temperature parameter of $T_{rot} = (1530 \pm 150)$ K.

Such a Boltzmann distribution cannot be expected *a priori*, because a selective photofragmentation process should provide a nonstatistical distribution. However, many chemical reactions and photodissociation processes yield products which show a Boltzmann distribution of the rotational states.[30] For the lowest vibrational level of the parent molecule the wave function is a Gaussian function of displacement coordinates. If there is no mechanism which selectively populates rotational states, then this Gaussian distribution of parent vibrational momentum is transformed into a Gaussian diatomic fragment rotational distribution characterized by a rotational temperature parameter.

C. OH vibrational distribution

We attempted to observe transitions in the $X^2\Pi(v''=1) \rightarrow A^2\Sigma(v'=1)$ band around 312 nm in order to determine the vibrational excitation of OH photofragment. However, no absorption lines could be assigned originating from vibrationally excited levels. From the noise and the OH transitions belonging to vibrationless levels in the $X^2\Pi$ state we determined an upper limit for OH products formed in $v'' = 1$. According to this procedure less than 2% of all OH fragments are vibrationally excited; an insignifi-

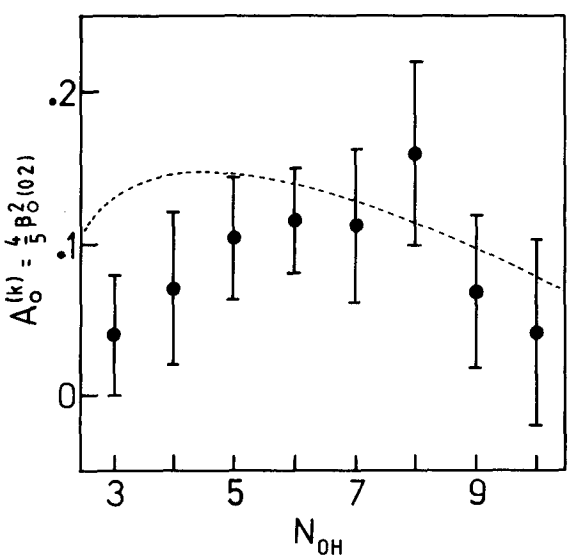

FIG. 3. The alignment parameter $A_0^{(2)}$ vs the angular momentum N_{OH} of the OH photofragment. No distinction had been made between the $^2\Pi_{3/2}$ and $^2\Pi_{1/2}$ spin systems. The dashed line results from a calculation on basis of a semiclassical dynamical model (see Sec. V C).

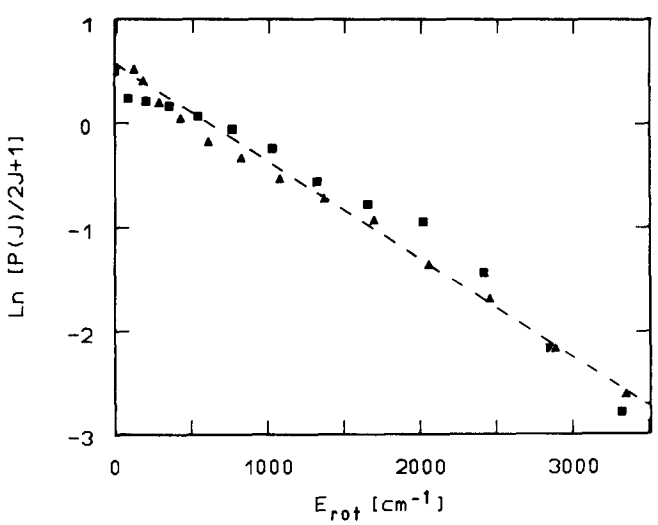

FIG. 4 OH rotational state populations $P(J)$ of the $^2\Pi_{3/2}$ levels (squares) and of the $^2\Pi_{1/2}$ levels (triangles) after dissociation of H_2O_2 at 266 nm. The rotational distribution is Boltzmannian characterized by a temperature parameter of $T_{rot} = 1530$ K.

cant amount in the overall mechanism of the photodissociation process of hydrogen peroxide at 266 nm.

D. Energy partitioning

The total excess energy E_{av} which is available for the $OH(X\,^2\Pi)$ photofragments is determined by the binding energy $E_d = 17\,300\ cm^{-1}$ ($\lambda_{threshold} = 578$ nm),[31] the photon energy ($h\nu = 37\,600\ cm^{-1}, \lambda = 266$ nm), and the initial internal energy $E_{in}(H_2O_2)$ of the H_2O_2 parent molecule

$$E_{av} = h\nu + E_{in}(H_2O_2) - E_d. \tag{5}$$

H_2O_2 is at thermal equilibrium at a temperature of $T = 300$ K.

Most of the vibrational energy of hydrogen peroxide originates from the ν_4 torsional mode (see Fig. 10). This mode contributes 85 cm^{-1} to $E_{in}(H_2O_2)$ while all other vibrational modes add only 15 cm^{-1} to the internal energy of H_2O_2. Thus we get for the internal excitation

$$E_{in}(H_2O_2) = E_{vib}(H_2O_2) + E_{rot}(H_2O_2) \cong 400\ cm^{-1} \tag{6}$$

and the total energy available for excitation of the two OH products is therefore

$$E_{av} = 20\,700\ cm^{-1}.$$

This energy is not sufficient to produce electronically excited OH fragments in the $A\,^2\Sigma$ state and in fact no $A \rightarrow X$ emission is observed. The fraction of this available energy partitioned into the various degrees of freedom is defined as

$$f_{rot} = \langle E_{rot}\rangle/E_{av};\quad f_{vib} = \langle E_{vib}\rangle/E_{av},$$
$$f_{trans} = \langle E_{trans}\rangle/E_{av} = 1 - f_{rot} - f_{vib}, \tag{7}$$

where the last equation is a consequence of conservation of energy. However, we also determined the translational energy by measuring the Doppler shift of recoiling OH photofragments.[19] From this observation we found that $(20\,000 \pm 1000)\ cm^{-1}$ is released as translational energy of the products corresponding to an OH recoil velocity of 3700 m/s.

The fact that most of the available energy is transferred into product translation is confirmed by the measurements concerning the internal excitation of OH fragment. Although, in principle, vibrational levels up to $v'' = 6$ can be populated, no vibrationally excited products could be found.

The rotational distribution is Boltzmannian and can be described by the temperature parameter $T_{rot} = 1530$ K corresponding to an energy of 1060 cm^{-1} for each OH fragment. Thus about 90% of the available energy is transferred into translational energy and less than 0.2% is converted into vibrational energy of the radicals. Consequently, the velocity distribution of recoiling OH photofragments must be quite narrow.

E. Spin distribution

The influence of the electron spin in the photodissociation of H_2O_2 has been determined by calculating the ratio of population numbers which represents the $^2\Pi_{3/2}$ state to those belonging to the $^2\Pi_{1/2}$ state. A plot of this ratio with appropriate statistical weights vs N_{OH} is shown in Fig. 5. A

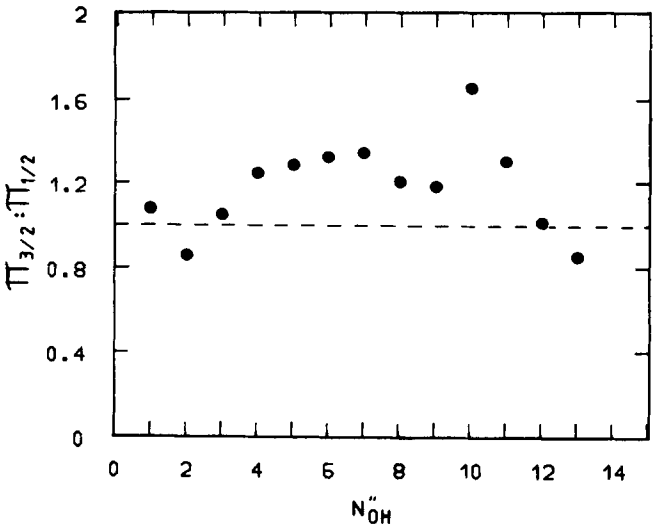

FIG. 5. Distribution of the spin components after photodissociation of hydrogen peroxide. Shown is the ratio of spin populations multiplied by the statistical weight as a function of N''_{OH}. The horizontal line at a value of unity indicates statistical distribution.

statistical distribution of the spin components would correspond to a straight line parallel to the abscissa with the intercept at $y = 1$. As can be seen from Fig. 5 no significant deviation from this line can be observed. Therefore, the dissociation process does not distinguish between the two spin-orbit states and the population is distributed statistically between the two spin components.

It should be mentioned that a rotational temperature distribution is not consistent with a complete statistical population of the two spin states. The $^2\Pi_{1/2}$ state lies at higher energies and consequently any rotational distribution which can be described by a positive temperature parameter will favor the $^2\Pi_{3/2}$ system.

F. Population of the Λ doublets

The fluorescence intensities of the Q and R branches were used to determine the Λ doublet state distribution of OH photoproduct. The origin of the Q lines is the upper Λ component (Π^-) while the lower Λ component (Π^+) is represented by the R lines. (The energetic ordering is reversed in the $^2\Pi_{1/2}$ levels for $N \leqslant 4$, for which Π^- lies below Π^+.)

Figure 6 shows the observed values of the ratio of the relative Λ doublet population $[(\Pi^-) - (\Pi^+)]/[(\Pi^-) + (\Pi^+)]$ as a function of the angular momentum J_{OH}. A statistical population between the two Λ components would be represented by a parallel line to the abscissa. A negative value would indicate a preference for the $\Pi^+(f_c)$ Λ state. We observe a positive value of $(Q - R)/(Q + R)$ indicating a small preferential population of the $\Pi^-(f_d)$ Λ doublet of OH.

This population inversion increases slightly with increasing J_{OH}. However, even at high J_{OH}, the preferential population of the Π^- state is well below the value found in the photodissociation of H_2O at 157 nm[8] and the single occupied $p\pi$ lobe does not show the maximum possible alignment.

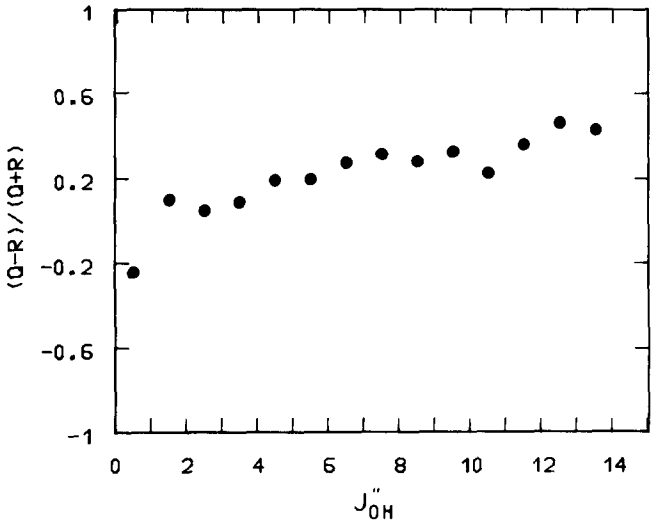

FIG. 6. Product state distribution between the two Λ doublets Π^+ and Π^- which were probed by R and Q transitions, respectively. Plotted is the ratio $(Q-R)/(Q+R)$ as a function of J''_{OH}. The observed small positive value indicates a preferential population of the upper Λ component.

IV. PHOTOFRAGMENT DOPPLER PROFILES

The transition moment of a photoselected parent molecule is preferentially aligned parallel to the electric field vector of the exciting polarized laser radiation. This anisotropy will be carried over to the photofragment motions, if the ejection of products is fast compared with the internal motions of the parent.

If the dissociation process is slow with respect to parent rotation during fragmentation the tangential velocity of the fragments during rotation may be comparable with the recoil velocity and influences the velocity of the products. Furthermore, if the dissociation is not instantaneous the anisotropic character of the dissociation process will be influenced by the ratio of the lifetime τ of the excited H_2O_2 parent to its rotational period.[19,32–34]

In the case of photodissociation of H_2O_2 at 266 nm the recoil velocity is very fast compared to H_2O_2 rotation and the dissociation process is sufficiently prompt not to influence strongly the anisotropic distribution of OH products. Thus the translational recoil and rotational anisotropy of the products will reflect the dynamical behavior of the photoselected H_2O_2 parent.

With narrow bandwidth tunable lasers and use of the sensitive laser-induced fluorescence technique the Doppler profiles of single quantum states can be probed. Using various polarization schemes for dissociations and probe lasers, these experiments can provide the three dimensional recoil velocity distribution of specific fragment states.[35] If the product is electronically excited then the rotational anisotropy can be determined from the polarization of the chemiluminescence.[22,23,36] For products formed in the electronic ground state, laser-induced fluorescence is used to determine rotational anisotropy by measuring relative intensities as a function of detection geometry and polarization of the analyzing laser beam.[9,10,25] Theories, which can be used to obtain the distribution of angular momentum from these polarization experiments, have been developed in different papers.[22,25–27,33]

However, these theoretical derivations describe only the correlation of the rotation with the alignment of the parent molecule transition moment or the correlation of the translational motion of the product with alignment. The correlation of rotational and translational motions with one another has been analyzed by Dixon.[37] This aspect of anisotropy is defined by the values of a number of bipolar moments of the translational and rotational angular distributions. These moments reflect the dynamics of the dissociation process and allow a deeper insight into the understanding of photodissociation mechanisms. The theory of Dixon contains detailed equations which show that the profile of a recoil Doppler broadened line of a fragment will depend on the polarization of the photolyzing and analyzing laser beams, the detection geometry, and the transition which is used for probing the photoproducts. In the following this formulation will be adopted and our intention is to show how these equations can be used to determine the bipolar moments and how their measurement provides detailed information about the reaction dynamics.

A. Analysis of Doppler broadened lines

The photofragments are probed with narrow bandwidth lasers. In sub-Doppler spectroscopy using LIF, the frequency which will be "seen" by the ejected product is shifted by the projection of its recoil velocity $\mathbf{v}$ onto the selected direction of the analyzing laser beam at angle θ. First we introduce x_D as the ratio of the displacement from line center $(\nu-\nu_0)$ to the maximum Doppler shift $\Delta\nu_D = \nu_0 v/c$,

$$x_D = \frac{\nu-\nu_0}{\Delta\nu_D}. \tag{8}$$

The range of x_D is limited from -1 to $+1$. The moments $A_q^{(k)}$ of the rotational distribution are expressed as functions of the relative Doppler shift x_D, and the generalized equation for a Doppler resolved spectral line is given by [see Eq. (19) in Ref. 37 and Eq. (1) in Ref. 25]

$$I(x_D,\theta) = CN_iS \sum_{k_d,k_a,k,q} A_q^{(k)}(J_i,x_D,\theta)\epsilon'(k_d,k_a,k,q;\Omega) \times \gamma'_{k_dk_ak}(J_i,J_e,J_f). \tag{9}$$

The quantities ϵ' and γ' are excitation–detection geometrical factors and angular momentum factors, respectively. N_i is the population of the initial state, S is the product of excitation $(i\rightarrow e)$ and emission $(e\rightarrow f)$ line strengths. The dependence of $A_q^{(k)}$ on x_D and θ is given in Table I of Ref. 37.

Inserting these functions into Eq. (9) the expression for the line profiles becomes inconveniently large. But in each case the line shape function can be written as

$$g(x_D) = \frac{1}{2\Delta\nu_D}\left[g_0 + g_2P_2(x_D) + g_4P_4(x_D) + g_6P_6(x_D)\right]. \tag{10}$$

Thus the line profiles have contributions from even Legendre polynomials up to the sixth order. However, one would expect a minor influence of the $P_4(x_D)$ and $P_6(x_D)$ terms on the observed line profiles. Indeed, calculated line profiles show that terms higher than $P_2(x_D)$ can easily be

missed in an experimental run, because of their negligible contribution. The intensity $I(x_D,\theta)$ is then given by

$$I/CN_iS = a_0[1 + \{2\beta_0^2(20)\}P_2(\theta)P_2(x_D)] + a_1[\tfrac{4}{5}\beta_0^2(02) + \{2\beta_0^0(22) - \tfrac{8}{7}\beta_0^2(22)\}P_2(\theta)P_2(x_D)]$$
$$+ a_2\{\tfrac{2}{3}\beta_0^0(22) + \tfrac{8}{21}\beta_0^2(22)\}[1 - P_2(\theta)]P_2(x_D) + a_3\{\tfrac{4}{7}\beta_0^2(24)P_2(\theta)\}P_2(x_D)$$
$$+ a_4\{\tfrac{2}{21}\beta_0^2(24)[1 - P_2(\theta)]\}P_2(x_D) + \cdots \quad (11)$$

with $P_2(x_D) = \frac{1}{2}(3x_D^2 - 1)$ and $P_2(\theta) = \frac{1}{2}(3\cos^2\theta - 1)$.

The parameters a_i can be calculated from the excitation–detection geometry factors ϵ' and the angular momentum coupling factors γ'.

As can be seen from Eqs. (10) and (11) the g_0 and g_2 terms are a linear combination of bipolar moments β_0^k,

$$g_0 = b_0 + b_1\beta_0^2(02),$$
$$g_2 = b_2\beta_0^2(20) + b_3\beta_0^0(22) + b_4\beta_0^2(22) + b_5\beta_0^2(24), \quad (12)$$

where the multipliers b_i of the bipolar moments are a linear combination of the parameters a_i in Eq. (11).

We used eight excitation–detection geometries for LIF analysis of the OH photofragment as described in the experimental section of this paper (Fig. 1). The undispersed fluorescence was always detected at right angles to the propagation direction of both the photolyzing and analyzing laser beams. Since no polarizer for the detected fluorescence light was used we have to take the mean of two of the cases as defined in Table III of Ref. 37. Then we get the six *different* geometries (I–VI)

$$\begin{aligned}
&\text{I. } H_p,H_a && = \tfrac{1}{2}(\text{case 1} + \text{case 2}),\\
&\text{II. } V_p,H_a;V_p',H_a && = \tfrac{1}{2}(\text{case 11} + \text{case 12}),\\
&\text{III. } H_p,V_a && = \tfrac{1}{2}(\text{case 3} + \text{case 4}),\\
&\text{IV. } V_p,V_a;V_p',V_a && = \tfrac{1}{2}(\text{case 9} + \text{case 10}),\\
&\text{V. } H_p',H_a && = \tfrac{1}{2}(\text{case 7} + \text{case 8}),\\
&\text{VI. } H_p',V_a && = \tfrac{1}{2}(\text{case 5} + \text{case 6}).
\end{aligned} \quad (13)$$

In cases I–IV the angle θ is $\pi/2$ and otherwise $\theta = 0$.

In Table I the numerical values of the multipliers b_0 to b_5 of the bipolar moments $\beta_0^{(k)}$ are listed for the six different geometries I–VI and selected transitions. The fact of observing undispersed fluorescence and depolarization by hyperfine precession has been taken into account. The multiplier b_5 in Table I is always one order of magnitude smaller than b_0–b_4 and consequently the influence of the corresponding moment on the observed line profiles will be negligibly small. Therefore, we did not attempt to determine this moment.

TABLE I. Examples of the multipliers b_0 to b_5 of the bipolar moments for the six geometries I–VI used in Eqs. (12) and (16).

	I	II	III	IV	V	VI
$P_1(2)$	0.9937	0.9937	1.0126	1.0126	0.9937	1.0126
or	−0.5703	0.2498	0.3047	−0.6095	0.3204	0.3047
$^oP_{12}(3)$	−0.9937	−0.9937	−1.0126	−1.0126	1.9874	2.0251
	0.8011	0.8011	0.7619	0.7619	0.8011	0.7619
	−0.3569	0.8147	0.8707	−0.4353	−0.4578	−0.4353
	−0.0052	−0.0052	0.0105	−0.0418	0.0105	0.0314
$Q_1(4)$	1.0460	1.0460	0.9081	0.9081	1.0460	0.9081
or	0.8182	−0.4273	−0.3098	0.6197	−0.3909	−0.3098
$^pQ_{12}(5)$	−1.0460	−1.0460	−0.9081	−0.9081	2.0919	1.8161
	−0.9771	−0.9771	−0.7746	−0.7746	−0.9771	−0.7746
	0.6104	−1.1688	−0.8852	0.4426	0.5584	0.4426
	0.0070	0.0070	−0.0139	0.0557	−0.0139	−0.0418
$P_2(5)$	0.9848	0.9848	1.0305	1.0305	0.9848	1.0305
or	−0.4888	0.1684	0.2867	−0.5733	0.3204	0.2867
$^qP_{21}(4)$	−0.9848	−0.9848	−1.0305	−1.0305	1.9695	2.0610
	0.8011	0.8011	0.7166	0.7166	0.8011	0.7166
	−0.2406	0.6984	0.8190	−0.4095	−0.4578	−0.4095
	−0.0073	−0.0073	0.0145	−0.0581	0.0145	0.0436
$Q_1(10)$	1.0494	1.0494	0.9013	0.9013	1.0494	0.9013
or	0.8663	−0.4623	0.3188	0.6377	−0.4040	−0.3188
$^pQ_{12}(11)$	−1.0494	−1.0494	−0.9013	−0.9013	2.0987	1.8026
	−1.0099	−1.0099	−0.7971	−0.7971	−1.0099	−0.7971
	0.6605	−1.2376	−0.9109	0.4555	0.5771	0.4555
	0.0087	0.0087	−0.0175	0.0700	−0.0175	−0.0525
$P_2(11)$	0.9786	0.9786	1.0427	1.0427	0.9786	1.0427
or	−0.4196	0.1162	0.2618	−0.5236	0.3034	0.2618
$^qP_{21}(10)$	−0.9786	−0.9786	−1.0427	−1.0427	1.9573	2.0855
	0.7586	0.7586	0.6545	0.6546	0.7586	0.6545
	−0.1660	0.5995	0.7481	−0.3740	−0.4335	−0.3740
	−0.0061	−0.0061	0.0122	−0.0489	0.0122	0.0367

The best method for the analysis of the moment $\beta_0^{(k)}$ is to fit the observed Doppler profiles to the function

$$g(x_D) \sim \frac{1}{2\Delta\nu_D}\left[1+\beta_{\text{eff}}P_2(\theta)P_2(x_D)\right] \tag{14}$$

with suitable convolution of the laser bandwidth and H_2O_2 parent molecule translational motion. (For details see Klee *et al.*[19]) The experimental values for β_{eff} which were obtained for different geometries and different branches have to be compared with the function

$$g(x_D) \sim \frac{g_0}{2\Delta\nu_D}\left[1+\frac{g_2}{g_0}P_2(x_D)\right]. \tag{15}$$

Thus for each branch we get six equations to determine the bipolar moments

$$\beta_{\text{eff}} = [b_2\beta_0^2(20) + b_3\beta_0^0(22) + b_4\beta_0^2(22)]/g_0P_2(\theta). \tag{16}$$

In the case of negligible alignment of photoproducts, Eq. (16) simplifies to

$$\begin{aligned}\text{I–IV: } \beta_{\text{eff}} &= 2\beta_0^2(20) - 2(b_3/b_0)\beta_0^0(22) \\ &\quad - 2(b_4/b_0)\beta_0^2(22), \\ \text{V–VI: } \beta_{\text{eff}} &= 2\beta_0^2(20) + (b_3/b_0)\beta_0^0(22) \\ &\quad + (b_4/b_0)\beta_0^2(22).\end{aligned} \tag{17}$$

Alignment of the fragments shows only an indirect influence on the line profile. The integral of the line profile depends only on g_0 and all terms in Eq. (11) within the brackets { } vanish

$$\int Id\nu/CN_iS = a_0 + a_1\tfrac{4}{5}\beta_0^2(02). \tag{18}$$

As can be seen from this equation the moment $\beta_0^2(02)$ is proportional to the usually defined alignment parameter $A_0^{(2)}$,

$$A_0^{(2)} = \tfrac{4}{5}\beta_0^2(02). \tag{19}$$

Therefore, we chose the most reliable method to obtain this simple alignment moment $\beta_0^2(02)$ by determining the integrated intensity ratios for lines in different geometries and branches. Then these values of $\beta_0^2(02)$ are used to determine the g_0 factor in Eqs. (15) and (16).

B. Evaluation of the bipolar moments $\beta_0^2(20)$, $\beta_0^0(22)$, $\beta_0^2(22)$

We observed more than 200 Doppler profiles from which detailed information concerning the correlation of translational and rotational motion of the products were extracted. Up to six different geometries were chosen to determine the bipolar moments and their dependence on rotation of the photofragment. As an example the recoil–Doppler broadened line profiles for the $Q_1(4)$ and $^qP_{21}(4)$ transitions are shown in Fig. 7. Doppler profiles were fitted in a least square fit procedure to the function (14) with a Gaussian convolution function of $\Delta\tilde{\nu} = 0.13\ \text{cm}^{-1}$ (FWHM).[19]

The $Q_1(4)$ Doppler broadened line shows a dip at geometry IV which becomes more flat at geometry III while the dip of the corresponding satellite line increases. At geometry VI the profiles look completely different, because in this case

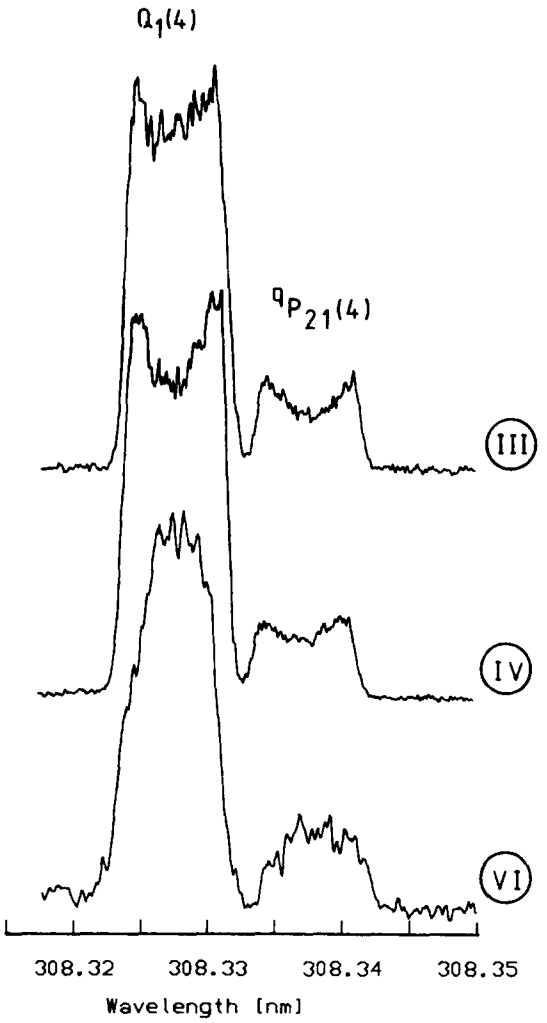

FIG. 7. High resolution excitation spectra in the region around the $Q_1(4)$ and $^qP_{21}(4)$ transitions for the three geometries III, IV, VI defined in Fig. 1.

most photofragments exhibit a velocity component which is nearly zero in the direction of the analyzing laser beam. Table II contains the measured value of β_{eff}(expt) for the six geometries. The strongest variation of β_{eff} is observed for geometry II or III when transitions of different branches, e.g., $Q_1(4)$ and $^qP_{21}(4)$, are used for the analysis. Also induced in Table II are the multipliers $b_i/g_0P_2(\cos\theta)$ which were used to determine the bipolar moments $\beta_0^2(20), \beta_0^0(22), \beta_0^2(22)$ in a least square fit procedure to Eq. (16).

The factor g_0 was calculated via Eq. (12) with the alignment moment $\beta_0^2(02) = 0.094$. But it should be mentioned that the influence of $\beta_0^2(02)$ on the evaluation of the other bipolar moments is not of importance in the photodissociation of H_2O_2 at 266 nm. This would be different in photofragmentation processes where strongly aligned products are formed.[11]

As can be seen from Table II the calculated β_{eff} values are in very good agreement with the experimental ones and the three bipolar moments $\beta_0^2(20), \beta_0^0(22)$, and $\beta_0^2(22)$ are sufficient to describe the 12 observed Doppler broadened line profiles.

TABLE II. Effective anisotropy parameter β_{eff} observed in the experiment and calculated using the listed multipliers for the $Q_1(4)$ main line and the accompanying ${}^qP_{21}(4)$ satellite line.

		Multipliers of $\beta^2_0(20), \beta^0_0(22), \beta^2_0(22)$			β_{eff}	
Line	Geom	b_2/x	b_3/x	b_4/x	Expt	Calc
$Q_1(4)$	I	1.8630	1.7403	−1.0872	−0.78	−0.78
	II	2.0799	1.9429	2.3240	−0.40	−0.36
	III	2.0663	1.7625	2.0142	−0.41	−0.41
	IV	1.8794	1.6031	−0.9160	−0.72	−0.77
	V	2.0727	−0.9681	0.5533	−0.65	−0.76
	VI	2.0661	−0.8812	0.5035	−0.76	−0.76
${}^qP_{21}(4)$	I	2.0979	−1.7066	0.5125	−0.82	−0.81
	II	1.9684	−1.6012	−1.3959	−1.02	−1.03
	III	1.9490	−1.3553	−1.5490	−1.09	−1.03
	IV	2.1104	−1.4675	0.8386	−0.79	−0.76
	V	1.9406	0.7893	−0.4511	−0.80	−0.76
	VI	1.9490	0.6777	−0.3873	−0.75	−0.76

$x = g_0 P_2(\cos\theta); \beta^2_0(02) = 0.094$

There are very close similarities between the line profiles for pairs of different geometries. This is because the multipliers b_i have approximately equal values; I≅IV, II≅III, V≅VI. The easiest experimental setup to realize these different geometries is a perpendicular arrangement between photolyzing and analyzing laser beam. On the other hand, the total fluorescence signal will be stronger if a counterpropagating configuration is chosen. The cases V and VI are also fairly insensitive geometries for measuring the bipolar moments, because of the low values of the multipliers b_3/x and b_4/x (Table II).

To measure the moment $\beta^2_0(22)$, geometries III and IV or I and II should be chosen, because b_4 changes its sign. Since b_3 changes also its sign when different branches, Q and P or Q and R, are used for LIF excitation a strong change in the observed Doppler profiles between main and satellite lines can also be expected.

We determined the rotational dependence of the bipolar moments by measuring the recoil Doppler broadened line profiles for different OH rotational states. With increasing N_{OH} the dip in the line profiles decreases for Q transitions with geometries II–III. Above $N_{\text{OH}} = 7$ the line shape parameter β_{eff} becomes positive. The highest OH rotational state we could use for an evaluation of the bipolar moments is $N_{\text{OH}} = 10$. The line profile of the $Q_1(10)$ transition is shown in Fig. 8. At higher N_{OH} it becomes more and more difficult to observe the ${}^qP_{21}$ satellite line because of decreasing transition probabilities and population numbers.

In Figs. 9(a)–9(c) the evaluated bipolar moments $\beta^2_0(20), \beta^0_0(22)$, and $\beta^2_0(22)$ are shown as function of the rotational motion of OH. The recoil anisotropy parameter β is proportional to the bipolar moment $\beta^2_0(20)$,

$$\beta = 2\beta^2_0(20). \tag{20}$$

Figure 9(a) shows this conventional β parameter as a function of N_{OH}. This parameter gives information on the symmetry, configuration, parent internal motion, and on the lifetime of the parent excited state. A detailed discussion of this parameter in terms of its meaning to understand the photodissociation dynamics of H_2O_2 is given by Klee *et al.*[19] We observe an N_{OH} independent β parameter with a mean value of $\beta = -0.71 \pm 0.08$. The small deviation of this value at $N_{\text{OH}} = 9$, 10 is probably caused by the weak (and noisy) satellite line which was also used to evaluate the bipolar moments.

All other β^k_0 parameters determine the correlation between translational and rotational motion of the OH fragment. For low values of J_{OH} specific quantum moments β^k_0 are zero for $J_{\text{OH}} < 1$. In the high J limit these quantum effects are less important and a semiclassical momentum representation provides a more direct physical interpretation.

The momentum $\beta^0_0(22)$ is a measure of the mutual correlation of the photofragment translational and rotational vectors $\mathbf{v}_{\text{OH}}$ and $\mathbf{J}_{\text{OH}}$, $[\beta^0_0(22) = P_2(v\cdot J)]$. It is independent on the frame of reference (lab or body fixed frame). The positive value of this moment at high J_{OH} indicates a bias

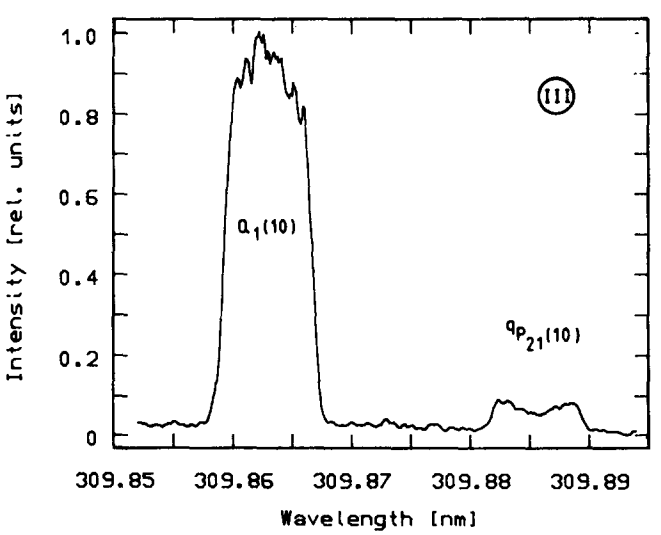

FIG. 8. Doppler profile of the $Q_1(10)$ main line and the accompanying ${}^qP_{21}(10)$ satellite line. The central dip of the Q transitions observed for low OH rotational excitation vanishes for high J_{OH} indicating a more parallel orientation of $\mathbf{J}_{\text{OH}}$ to $\mathbf{v}_{\text{OH}}$.

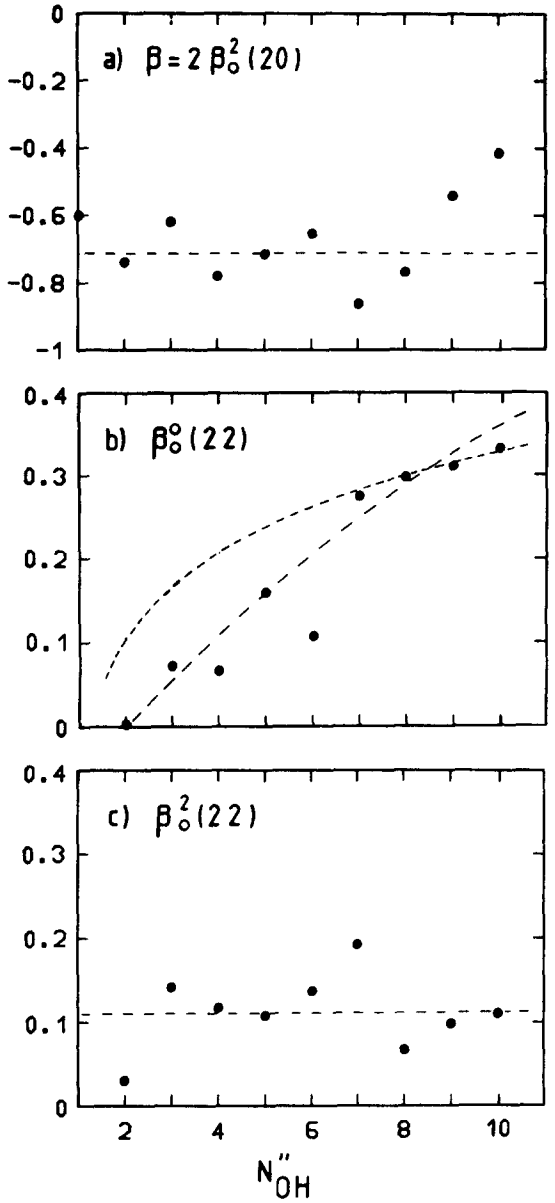

FIG. 9. Bipolar moments $\beta^2_0(20)$, $\beta^0_0(22)$, and $\beta^2_0(22)$ as a function of N''_{OH}. The conventionally defined anisotropy parameter β is proportional to the bipolar moment $\beta^2_0(20)$. Its large negative value indicates that the OH fragments are ejected essentially perpendicular to the transition dipole moment $\mu_{H_2O_2}$ of the parent molecule. The bipolar moment $\beta^0_0(22)$ is positive and increases with increasing rotation of the OH fragment indicating a more parallel orientation of $\mathbf{J}_{OH}$ to $\mathbf{v}_{OH}$. The bipolar moment $\beta^2_0(22)$ describes the correlation of the translational and rotational motion of the OH fragment and of the transition dipole moment $\mu_{H_2O_2}$ of the parent molecule. The long-dashed curves stem from fitting the experimental data, whereas the short-dashed one in (b) is calculated on basis of a semiclassical dynamical model (see Sec. V C).

towards $\mathbf{v}_{OH}$ and $\mathbf{J}_{OH}$ being parallel to one another. Its influence on the observed Doppler line profiles using LIF excitation can be understood as follows: the probability of excitation via Q transitions is highest when the electric vector $\mathbf{E}_a$ of the analyzing dye laser light is parallel to the rotational vector $\mathbf{J}_{OH}$ of the OH photofragment, and thus more parallel to $\mathbf{v}_{OH}$, because the positive value of $\beta^0_0(22)$ found for all $\mathbf{J}_{OH}$ implies a positive $\mathbf{v}_{OH}$–$\mathbf{J}_{OH}$ correlation. Since $\mathbf{E}_a$ is necessarily perpendicular to the photon progagation axis, this requires that the propagation axis be perpendicular to $\mathbf{v}_{OH}$, thereby resulting in a central maximum in the line profile. As $\beta^0_0(22)$ increases with increasing J_{OH}, this central maximum must also increase and consequently the central dip, found in the Q-line profile at low J_{OH}, has to vanish with higher OH rotation.

For P or R transitions the probability of excitation is highest with $\mathbf{E}_a$ perpendicular to $\mathbf{J}_{OH}$ and thus perpendicular to $\mathbf{v}_{OH}$, thereby enhancing the wings of the line profile over the center. Therefore, β_{eff} parameters of lower than -1 have been found, which should not be possible if β_{eff} would be interpreted as the conventionally defined anisotropy factor β [Eq. (1) of Ref. 19].

It is important to note that these effects associated with $\beta^0_0(22)$ depend *only* on the branch of the excitation transition, and are completely independent of beam geometries and polarization, as indicated by the spherical symmetry of β^0_0.

The moment $\beta^2_0(22)$ is a measure of the mutual correlation of the photofragment translational and rotational vectors ($\mathbf{v}_{OH}$,$\mathbf{J}_{OH}$) and of the transition dipole vector ($\mu_{H_2O_2}$) in the parent H_2O_2 molecule. We observed a low positive value of $\beta^2_0(22)$ for all J_{OH} [Fig. 9(c)] from which one gets $\beta^2_0(22) = 0.11 \pm 0.05$ as arithmetic mean.

In the following section the observed OH product state distribution and the evaluated bipolar moments will be discussed in terms of photodissociation dynamics of hydrogen peroxide.

V. DISCUSSION OF THE DISSOCIATION PROCESS

Hydrogen peroxide is the simplest molecule with hindered torsion about a single bond from which the influence of internal rotation on the dissociation process can be studied. Due to the only weakly hindered rotation, the geometry of warm H_2O_2 is quite variable and the excitation process may start from different locations on the ground state potential surface. First we will briefly describe the molecular structure of H_2O_2 in the electronic ground state (Fig. 10),

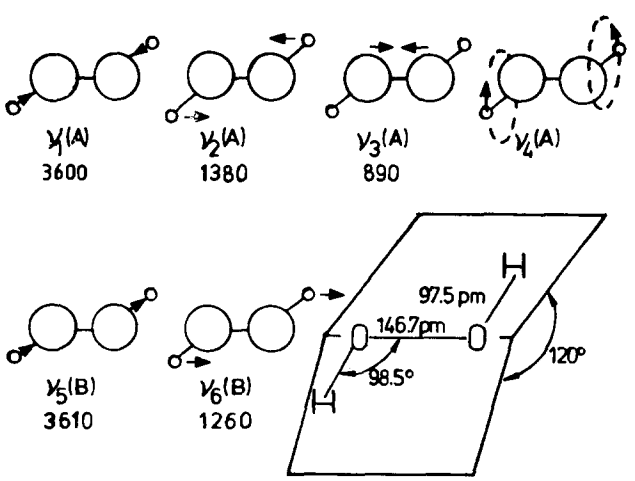

FIG. 10. Fundamental modes ν_1–ν_6, corresponding vibrational frequencies, and equilibrium configuration of the parent hydrogen peroxide molecule (Ref. 40). The energy levels which are related to the ν_4 torsional vibration are shown in Fig. 12.

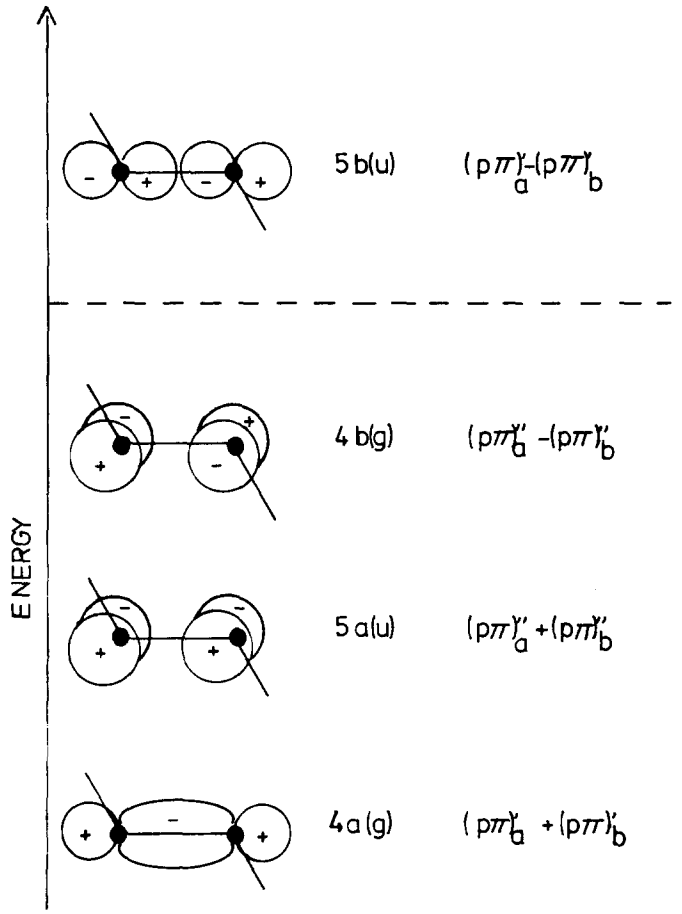

FIG. 11. Delocalized orbitals in an MO picture of (planar) H_2O_2. The highest occupied molecular orbital of the electronic ground state of H_2O_2 are $(4a_{(g)})^2(5a_{(u)})^2,(4b_{(g)})^2$. On excitation one of these electrons is promoted to the antibonding $(5b_{(u)})$ orbital. The prime or double prime indicates the symmetry of the $p\pi$ lobe in H_2O_2, while the subscript a or b at the $p\pi$ orbitals refers to one of the two OH radicals after fragmentation.

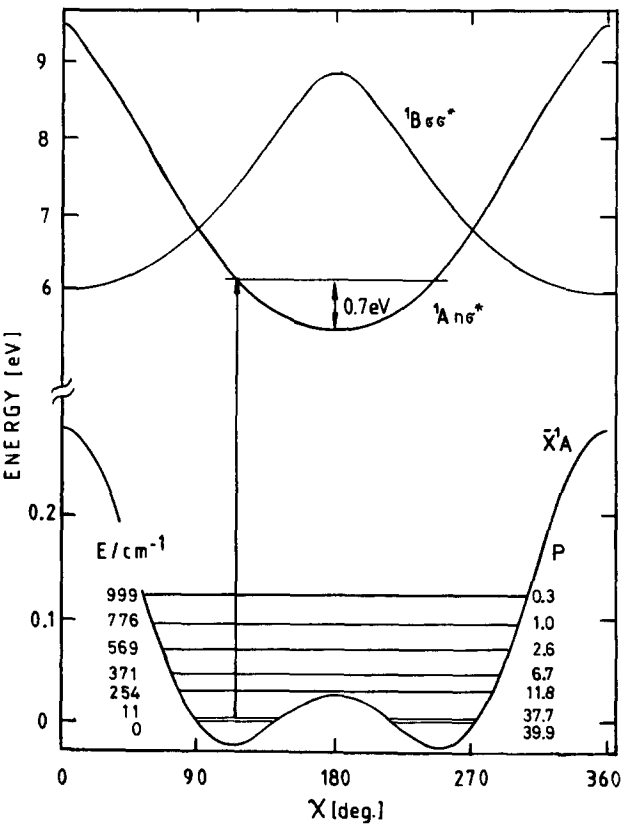

FIG. 12. Potential energy of H_2O_2 as a function of the torsion angle χ. The ground state potential function was evaluated on the basis of the hindered potential function (Ref. 38). The energy of the internal rotational states and their relative population numbers are also included. The potential energy function of the two electronic excited states, $\tilde{A}\,^1A$ and $\tilde{B}\,^1B$, were obtained by *ab initio* calculations (Ref. 42).

the electronic orbitals involved in the fragmentation process (Fig. 11), and the potential energy dependence of the internal rotation (Fig. 12) and the O–O internuclear distance (Fig. 13). This information together with the extensive experimental findings will then be used to discuss the photodissociation mechanism of hydrogen peroxide in detail.

A. Molecular structure of H_2O_2

Hydrogen peroxide with its skew configuration belongs to the point group C_2. Formation of planar H_2O_2 where the H atoms are in *cis* or in *trans* position ($\chi = 0$ or π) is hindered by potential barriers. The potential energy (in cm^{-1}) as a function of the dihedral angle χ can be described by[38]

$$V(\chi)/cm^1 = 993\cos(\chi) + 636\cos(2\chi) + 44\cos(3\chi) + 617. \quad (21)$$

The lower part of Fig. 12 shows the graph of $V(\chi)$. On the left of this curve the positions of the vibrational energy levels are indicated and to the right their relative populations P at $T = 300$ K.

According to Eq. (21) there is a very low potential barrier of $V_{trans} = (386 \pm 4)$ cm^{-1} for the *trans* position at $\chi = \pi$ and $V_{cis} = (2460 \pm 25)$ cm^{-1} for the *cis* position. The lowest energy level is 170 cm^{-1} above the potential minimum at $\chi_0 = 111.5°$.

Because of the narrow separation of the ground state doublet (11.4 cm^{-1}) both levels are nearly equally populated. Even the first excited state doublet at 254.2 and 370.7 cm^{-1}, just above the low *trans* barrier, is populated appreciably at the temperature of our measurements. For the lowest doublet, values of 118° and 114.3° were obtained as average dihedral angles between the two OH bonds.[38,39]

Figure 10 shows a schematic representation of the ground state configuration, the normal modes of H_2O_2 vibration and their energy in wave numbers.[40] The simplest way to describe the electronic states of hydrogen peroxide is the use of delocalized orbitals in an MO picture. For *trans*-planar H_2O_2 the electronic ground state $\tilde{X}\,^1A_{(g)}$ configuration is described by

$$\tilde{X}\,^1A_{(g)}...(4a_{(g)})^2(5a_{(u)})^2(4b_{(g)})^2.$$

On excitation one of these electrons is promoted to the antibonding $(5b_{(u)})$ orbital. The four orbitals involved in the dissociation process of hydrogen peroxide are shown in Fig. 11. The subscript a or b at the $p\pi$ orbitals in Fig. 11 refers to one of the two OH radicals after fragmentation, while the prime or double prime indicates the symmetry of the $p\pi$ lobe in H_2O_2. For separated OH radicals two orientations of this $p\pi$ lobe relative to the OH rotation plane are possible. In the high J limit these two orientations are identi-

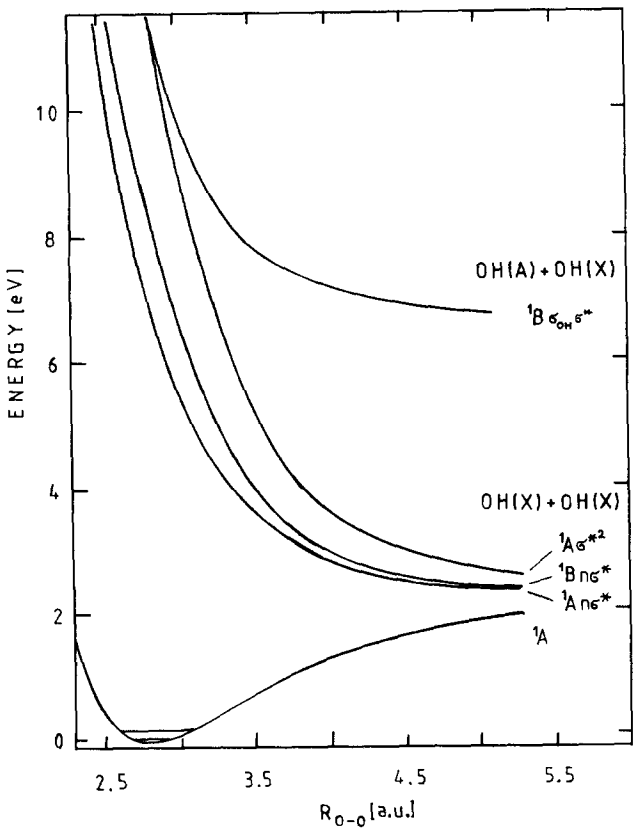

FIG. 13. Potential energy of H_2O_2 as a function of the O–O distance in hydrogen peroxide. The dependence of the energy of the electronic ground state $\tilde{X}\,^1A$ is described by a Morse function. The potential energy curves of the excited states, $\tilde{A}\,^1A$, $\tilde{B}\,^1B$, $\tilde{C}\,^1A$, were obtained by *ab initio* calculations (Ref. 42) and "normalized" to the ground state function at infinite O–O distance, where all curves describe two free OH radicals. All other coordinates were taken at the equilibrium configuration of H_2O_2.

fied by the two Λ doublet states Π^- and Π^+ (f_d and f_c following Herzberg's notation[21]).

The $\tilde{X}\,^1A$ state has 2 π' and $4\pi''$ electrons. Excitation from this state to the $\tilde{A}$ state ($n\sigma^*$) corresponds to a promotion of one of the two $4b_{(g)}$ electrons to the lowest antibonding orbital $5b_{(u)}$. Thus we get for the electronic configuration

$$\tilde{A}\,^1A_{(u)}\ldots(4a_{(g)})^2(5a_{(u)})^2(4b_{(g)})^1(5b_{(u)})^1$$

with 3 π' and 3 π'' electrons.

Dissociation from this state will therefore result in

$$HO_a(\pi')^2(\pi'')^1 + HO_b(\pi')^1(\pi'')^2$$

or

$$HO_a(\pi')^1(\pi'')^2 + HO_b(\pi')^2(\pi'')^1.$$

Thus in this simple picture one would not expect a dramatic difference in population between the two OH Λ doublets. If one OH is formed in a specific Λ state, then the partner molecule will be formed in the other corresponding Λ state and the observed sum of both OH fragments will not show a difference between the two Λ doublets.

The $\tilde{B}$ state ($n\sigma^*$) is reached by raising one $5a_{(u)}$ electron to the $5b_{(u)}$ orbital

$$\tilde{B}\,^1B_{(g)}\ldots(4a_{(g)})^2(5a_{(u)})^1(4b_{(g)})^2(5b_{(u)})^1.$$

Therefore, the $\tilde{B}$ state has 3 π' and $3\pi''$ electrons also.

When two $4b_{(g)}$ electrons are raised to the $5b_{(u)}$ orbital, then the resulting $\tilde{C}$ state $(\sigma^*)^2$ contains 4 π' and 2 π'' electrons

$$\tilde{C}\,^1A_{(g)}\ldots(4a_{(g)})^2(5a_{(u)})^2(5b_{(u)})^2.$$

Fragmentation from this state will yield

$$HO_a(\pi')^1(\pi'')^2 + HO_b(\pi')^1(\pi'')^2.$$

In this case the two Λ doublets should show a strong nonstatistical population distribution.

It goes without saying that this MO picture is a simplified view of hydrogen peroxide. On the other hand, from the OH photofragment angular distribution we know that a ^1A state is excited at 266 nm.[19] Two electronically excited states have ^1A symmetry. However, the $\tilde{C}\,^1A$ electronic state is caused by raising two electrons from a nonbonding to an antibonding orbital. Therefore, the $\tilde{C}\,^1A$ state will be much higher in energy than the $\tilde{A}\,^1A$ state. Since the excitation wavelength of 266 nm is at the edge of the absorption spectrum of H_2O_2,[15,31,41] we should observe OH products originating from the $\tilde{A}\,^1A$ electronic state. The proposed order of the electronic excited states is confirmed by *ab initio* calculations of Staemmler[42] and Chevaldonnet *et al.*[43]

The upper part of Fig. 13 shows the potential energy of the $\tilde{A}\,^1A$ ($n\sigma^*$), $\tilde{B}\,^1B$ ($n\sigma^*$), and $\tilde{C}\,^1A$ (σ^{*2}) states as function of the O–O distance for a torsional angle of 116° in H_2O_2.[42] The dependence of the energy of the electronic ground state $\tilde{X}\,^1A$ is described by a Morse function with the potential well depth of $D_e = 17\,790\ \text{cm}^{-1}$ for the reaction coordinate, an equilibrium distance of $r_0 = 147$ pm and a Morse parameter $a = 0.0238\ \text{pm}^{-1}$.

The potential energy curves of the excited states have been "normalized" to the ground state function at infinite O–O distance, where all curves describe two separated OH photofragments in the electronic ground state, $X\,^2\Pi$. This is an adequate procedure, because the experimentally determined ground state function is much more accurate than the calculated one, especially in terms of the well depth of the potential energy curve. For a direct Franck–Condon transition $\tilde{X}\,^1A(v_3'' = 0) \rightarrow \tilde{A}\,^1A$ a photon energy of roughly 7 eV is needed, which corresponds to the maximum of the H_2O_2 UV absorption spectrum.[15] Therefore, the excitation energy of 4.66 eV used in the photolysis of H_2O_2 is not sufficient to induce such a transition in the equilibrium geometry of hydrogen peroxide.

The potential energy of the electronic excited states $\tilde{A}\,^1A$ and $\tilde{B}\,^1B$ is strongly dependent on the torsion angle χ while the ground state shows only a minor energy dependence on χ. The upper part of Fig. 12 exhibits the potential energy of the electronic excited states ($\tilde{A}$ and $\tilde{B}$) as a function the dihedral angle χ at the O–O equilibrium distance. The $\tilde{B}\,^1B$ state has its minimum at the *cis* position of the two H atoms, whereas the $\tilde{A}\,^1A$ configuration has its maximum energy at this geometry. For planar H_2O_2 in the *trans* position the potential energy of the $\tilde{B}$ state is several eV higher than the energy of the $\tilde{A}$ state, which has its minimum in this position.

The three possible triplet states are not included in Figs. 12 and 13 because we do not expect to excite any of these states starting from the $\tilde{X}\,^1A$ ground states as a consequence of vanishing transition probabilities.

B. Mechanism for the photodissociation of H_2O_2

We do not observe any vibrationally excited OH photoproducts. The Franck–Condon principle[44] and the sudden model[45] explain the observation of vibrationally cold OH photofragments. The equilibrium bond length of OH in the parent hydrogen peroxide molecule is 97 pm. This value is comparable with the one in the OH molecule, $r_{OH} = 101.2$ pm. The same is true for the OH stretching frequencies (3600 and 3610 cm^{-1}; Fig. 10) in H_2O_2 and the vibrational frequency of the free radical (3735 cm^{-1}).[46] This implies, similarly to the photodissociation of HONO,[9,47] that the Franck–Condon factors for the decomposition of H_2O_2 to OH are diagonal, suggesting a fragmentation into vibrationless products.

A simple impulsive model also predicts essentially no vibrational excitation in the fragments.[48] The HOO angle (see Fig. 10) is close to 90° and any impulse along the O–O axis has only a small component along the O–H bond axis.

All three models mentioned above, predict vibrationally cold OH fragments in case of the photodissociation of hydrogen peroxide and water. But the photolysis of water at 157 nm in its first absorption band yields vibrationally excited OH products.[8] In this case an electron is raised from the nonbonding $1b_1$ to an antibonding $4a_1^*$ orbital in H_2O resulting in an excitation of the symmetric stretch. One H atom leaves the $\tilde{A}\ ^1B_1$ state and vibrational energy remains in the OH fragment. In contrast to the photodissociation of water the excitation of H_2O_2 to the $\tilde{A}\ ^1A$ state is an $n\sigma^*$ transition where only the O–O bonding electrons are involved.

Thus the upper electronic surface $\tilde{A}\ ^1A$ shows only a small change in the dependence of the potential energy on the OH distance in H_2O_2. Consequently this bond will not be compressed or stretched and practically no vibrational excitation of the OH photoproducts will occur.

The only internal energy of the OH fragments that we could observe in the photodissociation of H_2O_2 at 266 nm is the relatively low rotational excitation. The possible sources of this product rotation are parent molecule rotation, the torque from an impulse along the O–O bond, motion initially present as parent molecule vibration, and any additional torque generated by an angular dependence of the excited state potential energy surface.

Since the parent molecule is not internally cold, ground state rotation of the hydrogen peroxide will result in some OH rotation. Under this assumption, the OH rotation will mainly originate from rotation of H_2O_2 around the a axis, which is approximately parallel to the O–O bond. If the mean angular velocity of OH in the parent is transferred to the *two* OH fragments, then this mechanism amounts to less than 40 cm^{-1} of rotational energy for each OH. Obviously, this mechanism makes a very small contribution to the observed rotational excitation.

The second possible source for OH rotation could be the repulsive force between the two OH fragments during the dissociation. An impulse directed along the central O–O bond would not act through the OH centers of mass, and would therefore induce a torque on the O atoms in H_2O_2 which would be observable as OH rotation after the fragmentation. This model[48] assumes that the OH is regarded as a rigid rotor such that the H atom would follow the torque exerted on the oxygen atom. A maximum of 3% (620 cm^{-1}) of the available energy (20 700 cm^{-1}) in the dissociation process will thus appear as OH rotation. This rotational energy corresponds to $N_{OH} \sim 5$, but the rotational distribution should be non-Boltzmannian and relatively sharply peaked around this value. Since we do not observe such a distribution the main origin of the OH rotation cannot be explained by an impulsive model. Furthermore, such a mechanism would lead to a *large* positive alignment, in contrast to the low value observed.

A further source of product rotation is the vibrational motion in the parent H_2O_2. There are three vibrational modes which can be responsible for product rotation: the ν_2 OOH symmetric bend (1380 cm^{-1}), the ν_6 OOH asymmetric bend (1266 cm^{-1}), and the ν_4 torsion mode (Figs. 10 and 12). All these vibrational modes (ν_2,ν_6, and ν_4) induce an angular momentum in the OH fragment.

At room temperature, the parent ν_2 and ν_6 bending vibrations are not excited. Therefore, only the zero point energy of both vibrations (1323 cm^{-1}) has to be distributed between the *two* OH products. The OH fragments can take almost 50% of this vibrational energy as rotational energy.[16,49] Consequently *each* OH receives 330 cm^{-1} as rotational energy originating from the ν_2 and ν_6 modes.

Before we discuss the influence of the ν_4 torsional vibration on the rotational distribution we have to consider that the H_2O_2 excitation takes place at the long wavelength edge of the absorption spectrum. The applied energy of 4.66 eV is not sufficient to excite H_2O_2 from its equilibrium geometry. The potential energy of the $\tilde{A}\ ^1A$ electronic excited state is strongly dependent on the O–O distance in the hydrogen peroxide molecule, as would be expected for a dissociation process where most of the available energy is transferred into translational motion. But even at the classical turning point of $v_3'' = 0$ where $|\langle\psi|\psi\rangle|$ is already very small, an excitation energy of more than 6 eV is needed to reach the $\tilde{A}$ state. The situation is similar for an excitation $\tilde{X}\ ^1A(v_3'' = 1) \rightarrow \tilde{A}\ ^1A$, from the very weakly populated ($P \cong 1\%$) ν_3O–O stretching vibrational excited level. In this case more than 5 eV is needed at the classical turning point of large O–O distance.

The only other coordinate on which the potential energy of H_2O_2 ($\tilde{A}$,$\tilde{B}$) strongly depends, is the torsion angle χ. The potential energy of the ^1A electronic excited state has its minimum at the *trans* position ($\chi = 180°$) of the H atoms. At $\chi = 180°$ the ground state function exhibits a local maximum. However, this energy barrier is very low and more than 22% of all H_2O_2 parent molecules populate vibrationally excited levels of the ν_4 internal torsion mode. Therefore, it seems to be most likely that the excitation process of H_2O_2 at 266 nm starts to an appreciable extent from ν_4 vibrationally excited levels in a nearly planar parent molecule. If this assumption is valid, then the absorption cross section of H_2O_2 should be temperature dependent in this wavelength range. Indeed, Kijewski and Troe[50] found a significant temperature dependence of σ at $\lambda > 220$ nm. At the wavelength of 266 nm they determined absorption cross sections of $\sigma = 4.3\times10^{-20}$, 7.6×10^{-20}, and 13×10^{-20} cm^2 for the temperature 300, 600, and 1100 K, respectively. At $\chi = 180°$

almost all the torsional energy is transferred to OH product rotation. We assume that up to 700 cm^{-1} of OH product rotation originates from H_2O_2 torsion, either directly from excitation into the initial level, or from the torque provided by the strong angular dependence of the $\tilde{A}$ state potential (Fig. 12).

A Gaussian distribution of parent bending or torsion vibrational momentum is transformed into a Gaussian diatomic fragment rotational distribution.[49] The overall rotational distribution is thus characterized by a Boltzmann distribution with a "rotational temperature parameter." A total energy of 330 cm^{-1} from bending and 700 cm^{-1} from torsional motion will result in two temperature parameters. However, the experimentally observable overall distribution will show only a very small and negligible deviation from a straight line in a Boltzmann plot with a single parameter of $T_{rot} \cong 1500$ K.

We observe an increasing population of the upper Λ component with increasing OH rotation. This population inversion is not as dramatic as in the photolysis of H_2O at 157 nm[8,51] but the simple MO picture predicts no preference of a Λ state when H_2O_2 is excited to the $\tilde{A}\ ^1A$ state. However, fragmentation from the $\tilde{C}\ ^1A$ state would result in $4\pi'$ and $2\pi''$ electrons. The $\tilde{A}\ ^1A_{(g)}$ and $\tilde{C}\ ^1A_{(u)}$ states cannot mix by configuration interaction if H_2O_2 is planar, but excitation of the torsional mode may influence the final electronic state and differences in the population of the two Λ levels become possible within the presented MO picture.

We will now discuss the observed values of the bipolar moments. The recoil anisotropy parameter $\beta = 2\beta_0^2(20)$ was found to be independent of J_{OH}. Its negative value of -0.71 indicates that the OH translational distribution peaks in a direction perpendicular to the polarized dissociating laser light. This proves that the transition dipole moment ($\boldsymbol{\mu}_{H_2O_2}$) is essentially perpendicular to the O–O axis in hydrogen peroxide, as expected for a $^1A_{(u)} - {}^1A_{(g)}$ transition. Deviation from the limiting value of $\beta = -1$ is caused by internal motion of H_2O_2 and its overall rotation during the finite lifetime ($\leqslant 60$ fs) of the excited electronic state.[19] A finite dissociation lifetime will not affect the spherically symmetric bipolar moment $\beta_0^0(22)$ compared with prompt dissociation, but will reduce the values of all the $\beta_0^2(k_1k_2)$ moments—though not all to the same extent because of the different rotational velocities about the three axes of H_2O_2.

We define a coordinate system where $\boldsymbol{\mu}_{H_2O_2}$ is oriented along the z axis, with the O–O axis perpendicular to z such that the recoiling OH fragments will move along the x axis. Three limiting orientations of $\mathbf{J}_{OH}$ relative to $\boldsymbol{\mu}_{H_2O_2}$ and $\mathbf{v}_{OH}$ are possible (a) $\mathbf{J}_{OH}$ is perpendicular to both $\boldsymbol{\mu}_{H_2O_2}$ and $\mathbf{v}_{OH}$ and thus along the y axis, (b) $\mathbf{J}_{OH}$ parallel to $\boldsymbol{\mu}_{H_2O_2}$ along the z axis, or (c) $\mathbf{J}_{OH}$ parallel to $\mathbf{v}_{OH}$ along the x axis. Table III shows the limiting values of the bipolar moments for these three cases, and the comparison with the observed moments in the present experiment. Since we find positive values for the three bipolar moments $\beta_0^2(02)$, $\beta_0^0(22)$, and $\beta_0^2(22)$ the major components of $\mathbf{J}_{OH}$ must be J_x and J_z, with a very small component along the y axis which is perpendicular to both $\mathbf{v}_{OH}$ and $\boldsymbol{\mu}_{H_2O_2}$. Thus, for high J at least,

$$\langle J_y^2 \rangle \ll J(J+1).$$

TABLE III. The values of the lower order of bipolar moments for the three limiting orientations of v and J of the OH photofragment with v perpendicular to $\mu_{H_2O_2}$. The last column shows the experimental observed moments for high J_{OH} (experimental error ± 0.04).

	$\beta_0^2(20)$	$\beta_0^2(02)$	$\beta_0^0(22)$	$\beta_0^2(22)$
$\hat{y} = \mathbf{J} \perp \boldsymbol{\mu}, \mathbf{v}$	-0.5	-0.5	-0.5	-1.0
$\hat{z} = \mathbf{J} \parallel \boldsymbol{\mu}$	-0.5	$+1.0$	-0.5	$+0.5$
$\hat{x} = \mathbf{J} \parallel \mathbf{v}$	-0.5	-0.5	$+1.0$	$+0.5$
Observed	-0.36	$+0.09$	$+0.35$	$+0.11$

OH rotation may originate from the vibrational motion in the parent H_2O_2. The component of $\mathbf{J}_{OH}$ along the x axis should arise from ν_4 torsion ($\mathbf{J}_{OH}$ parallel to $\mathbf{v}_{OH}$). The J_z and J_y components are a result of the bending motions ν_2 and ν_6. For planar H_2O_2 where the H atoms are in *trans* position and perpendicular to the transition moment $\boldsymbol{\mu}_{H_2O_2}$ one would find the bending component of $\mathbf{J}_{OH}$ parallel to $\boldsymbol{\mu}_{H_2O_2}$ along the z axis, while $\mathbf{J}_{OH}$ would be oriented along the y axis if planar H_2O_2 fragments with the H atoms in *cis* position and parallel to $\boldsymbol{\mu}_{H_2O_2}$. Consequently only the J_x and J_z components need to be considered in the following and fragmentation of essentially planar H_2O_2 with the H atoms in *trans* position is the most likely process.

An orientation of the OH angular momentum along the z axis ($\mathbf{J}_{OH}$ perpendicular to $\mathbf{v}_{OH}$) would result in a negative value of the bipolar moment $\beta_0^0(22)$, while a positive value would indicate an orientation of $\mathbf{J}_{OH}$ along the x axis and parallel to $\mathbf{v}_{OH}$. We find an increasingly positive value of $\beta_0^0(22)$ with increasing $\mathbf{J}_{OH}$ indicating an orientation of $\mathbf{J}_{OH}$ more and more parallel to the axis of recoiling OH photofragments.

In the high J limit the bipolar moment $\beta_0^2(02)$ is the expectation value of $2\langle P_2(\cos\theta_r)\rangle$ with θ_r being the final angle between the $\mathbf{J}_{OH}$ vector of OH and the body fixed $\boldsymbol{\mu}$ vector of H_2O_2. The bipolar moment $\beta_0^0(22)$ is given in a semiclassical picture as the expectation value of $2\langle P_2(\cos\theta_{tr})\rangle$, where θ_{tr} is the angle between $\mathbf{v}_{OH}$ and $\mathbf{J}_{OH}$ of the recoiling OH product. In the coordinate system defined above, with $\boldsymbol{\mu}_{H_2O_2}$ and $\mathbf{v}_{OH}$ mutually orthogonal, these expressions can be written as

$$\beta_0^0(22) = \frac{2\langle J_x^2\rangle - \langle J_y^2\rangle - \langle J_z^2\rangle}{2J(J+1)}, \tag{22}$$

$$\beta_0^2(02) = \frac{2\langle J_z^2\rangle - \langle J_y^2\rangle - \langle J_x^2\rangle}{2J(J+1)}. \tag{23}$$

For $\beta_0^2(02)$ we observed a low mean value of 0.09, while $\beta_0^0(22)$ does not reach the maximum value possible in the high J limit. We assume a high J value of $\beta_0^0(22) \cong 0.41$. Since $\langle J_y^2\rangle \sim 0$ we get

$$\beta_0^0(22) + \beta_0^2(02) \leqslant 0.5$$

which also satisfies the relation

$$\langle J_x^2\rangle + \langle J_z^2\rangle \leqslant J(J+1). \tag{24}$$

Then the expectation values of the square of the angular momentum components are given by

$$\langle J_x^2\rangle \sim 0.61J(J+1),$$

$$\langle J_y^2 \rangle \sim 0,$$
$$\langle J_z^2 \rangle \sim 0.39J(J+1). \quad (25)$$

On the first view it might be surprising that one observes a strong correlation of $\mathbf{J}_{OH}$ with $\mathbf{v}_{OH}$ and of $\mathbf{v}_{OH}$ with $\boldsymbol{\mu}_{H_2O_2}$, but almost no correlation of $\mathbf{J}_{OH}$ with $\boldsymbol{\mu}_{H_2O_2}$. However, these correlations are not completely perfect. Therefore, the observed tendency of $\mathbf{J}_{OH}$ being parallel to $\mathbf{v}_{OH}$ is not a hint that the expectation values of both angular momentum components $\langle J_y^2 \rangle$ *and* $\langle J_z^2 \rangle$ are negligible. It is really just $\langle J_y^2 \rangle$ that is very small, while $\langle J_z^2 \rangle$ has to be taken into account [Eq. (25)].

Strictly speaking, to obtain $\langle J_x^2 \rangle$ and $\langle J_z^2 \rangle$ one should use the mean value $\langle \beta_0^0(22) \rangle$ of the J dependent moment. We now examine this J dependence in the light of a theoretical model.

C. A semiclassical dynamical model

The above conclusions suggest a dynamical model which is similar to that used in interpreting the angular momentum distribution in the OH radical from HONO photolysis,[9] but is not identical with it. We use a Hund's case (b) approximation, and assume that the nuclear rotational angular momentum **R** is initially generated in a plane perpendicular to the OH bond of planar *trans* H_2O_2; i.e., in a plane at $\alpha = 90°$ to the xz plane.[52] The components of **R** parallel and perpendicular to z ($R_\parallel$ and $R_\perp$, respectively) are each given Gaussian distributions with mean energies $\langle E_\parallel \rangle$ and $\langle E_\perp \rangle$, giving an overall distribution function

$$f(R) = (\rho_\parallel \rho_\perp)^{1/2} \pi^{-1} \exp\{-\rho_\parallel R_\parallel^2 - \rho_\perp R_\perp^2\}, \quad (26)$$

where

$$\rho_\parallel = B_{OH}/\langle E_\parallel \rangle,$$
$$\rho_\perp = B_{OH}/\langle E_\perp \rangle. \quad (27)$$

R is the component perpendicular to the OH bond of the rotational angular momentum **N** for which the parallel component is **Λ**, with $\Lambda = 1$.

Rotating to the xyz frame

$$N_x = R_\perp \cos\alpha + \Lambda \sin\alpha,$$
$$N_y = \Lambda \cos\alpha - R_\perp \sin\alpha, \quad (28)$$
$$N_z = R_\parallel.$$

For each value of the N quantum number the moments $\beta_0^0(22)$ and $\beta_0^2(02)$ are calculated as in Eqs. (22) and (23) using numerical integration over the angular distribution of **N**. Finally we note that **N** and **S** are coupled to give the resultant $\mathbf{J}_{OH}$ so that **N** will precess rapidly about $\mathbf{J}_{OH}$. This leads to a slightly lower alignment for $\mathbf{J}_{OH}$ than for **N**, such that for all levels of a Hund's case (b) doublet state

$$\frac{\beta_0^0(22)_J}{\beta_0^0(22)_N} = \frac{\beta_0^2(02)_J}{\beta_0^2(02)_N} = \left[1 - \frac{3}{4J(J+1)}\right]. \quad (29)$$

The mean energies $\langle E_\parallel \rangle$ and $\langle E_\perp \rangle$ were varied, subject to the constraint from the observed population distribution that their sum is 1065 cm^{-1}, until the value of $\beta_0^0(22)$ agreed with experiment for $N = 10$, the highest value observed. This leads to

$$\langle E_\parallel \rangle = (450 \pm 25)\ cm^{-1},$$
$$\langle E_\perp \rangle = (615 \pm 25)\ cm^{-1}, \quad (30)$$

in the ratio 0.42:0.58, which is close to the value deduced in Eq. (25). In addition, this calculation leads to the correct order of magnitude for $\beta_0^2(02)$, and reproduces the general trend with J_{OH} for both these moments [Figs. 3 and 9(b)]. Furthermore, the Boltzmann plot for this calculated distribution shows negligible curvature, despite the inclusion of two different Gaussian exponents.

Even so, this model is not quantitatively accurate. Both $\beta_0^0(22)$ and $\beta_0^2(02)$ are too large at low N_{OH}, which we attribute to the inadequacy of Hund's case (b) and semiclassical theory for these levels. $\beta_0^2(22)$ is considerably overestimated at all N_{OH}, but we expect this moment to be most affected by a finite dissociation lifetime.

The value of $\langle E_\parallel \rangle$ is noticeably greater than the estimate of 330 cm^{-1} derived solely from the zero point energy of the bending vibrations. The impulse of the dissociation must therefore contribute about 100 cm^{-1} to the energy of rotation about the z axis, but without significantly distorting the Gaussian distribution. $\langle E_\perp \rangle$ is sufficiently large that much of this energy must have been generated by torsional motion on the excited state surface. This potential is approximately quadratic in χ around $\chi = 180°$ (Fig. 12). Thus in an IOSA quantum treatment of the fragmentation[53] the ground state wave function will be multiplied by a phase factor $\exp\{-ia(\chi - \pi)^2\}$. This will increase the torsional kinetic energy over that present in the initial state, but will preserve a Gaussian distribution provided that dissociation takes place from near planar geometries.

These conclusions are in excellent agreement with the observed rotational distribution, but, in addition, we have obtained information about the relative orientations of $\boldsymbol{\mu}_{H_2O_2}$, $\mathbf{J}_{OH}$, $\mathbf{v}_{OH}$, and the origin of the OH angular momentum.

An evaluation of the recoil Doppler broadened line profiles at different experimental geometries was simplified by the fact that the OH product molecules are generated with a small internal excitation resulting in a very narrow distribution of translational recoil velocities. In principle, a broad velocity distribution can be determined by forming a weighted mean of the profiles for the various geometries and branches.[10,11] In practice, however, this technique cannot be recommended, because in the presence of noise, the necessary mathematical procedures, such as deconvolution and differentiation, will magnify this noise enormously.

VI. CONCLUSIONS

We have measured the scalar and vectorial properties of the photodissociation of hydrogen peroxide in considerable detail using polarization and sub-Doppler laser spectroscopic techniques. The complete nascent internal state distribution, alignment, translation, and correlations between the translational and internal motions of OH photoproducts and the transition dipole moment of the parent H_2O_2 have been

determined. The experimental results are:

(1) The photoproducts are formed in the OH $X\,^2\Pi_{3/2,\,1/2}$ state; two photon excitation in H_2O_2 has not been observed at the photolysis wavelength of 266 nm.

(2) The excess energy of 248 kJ/mol is preferentially transferred into OH recoil; 90% of the available energy is transformed into translation, 10% into rotation, and $<0.2\%$ into vibration.

(3) The OH rotational distribution can be described by a Boltzmann distribution with a temperature parameter of (1530 ± 150) K.

(4) No vibrationally excited OH was found.

(5) The two spin states are populated nearly statistically.

(6) The Λ doublets show a small inversion which increases with increasing OH rotation.

(7) The profiles of recoil Doppler broadened spectral lines are strongly dependent on the nature of the transition, on the excitation–detection geometry, and on the polarization of dissociating and analyzing laser light in contrast to the line intensities which show only a small dependence.

(8) The alignment parameter was found to be very small, $A_0^{(2)} = \frac{4}{5}\beta_0^2(02) \leqslant 0.1$.

(9) The bipolar moment $\beta_0^2(20)$ corresponds to the conventional defined anisotropy parameter $\beta = 2\beta_0^2(20)$ and describes the mass fragment angular distribution. Its value was found to be $\beta = -0.71 \pm 0.08$.

(10) The angular distribution peaks in the direction perpendicular to the electric field vector of the dissociating light.

(11) The transition induced in H_2O_2 is

$$\tilde{X}\,^1A + h\nu \rightarrow \tilde{A}\,^1A\,[(4a_{(g)})^2(5a_{(u)})^2(4b_{(g)})^1(5b_{(u)})^1].$$

(12) The moment $\beta_0^0(22)$, describing the vector correlation between the translational and rotational motions of the fragment, increases with increasing J_{OH}, indicating a bias towards $\mathbf{v}_{OH}$ and $\mathbf{J}_{OH}$ being parallel to one another.

(13) The moment $\beta_0^2(22)$ is a measure of the mutual correlation of the fragment translational and rotational vectors and the transition dipole vector in the parent molecule. The observed positive values of this moment, $\beta_0^2(22) = 0.11$, and of the moments $\beta_0^0(22)$ and $\beta_0^2(02)$ indicate that the expectation value of $\langle J_y^2 \rangle$ should be very small when $\boldsymbol{\mu}_{H_2O_2}$ defines the z axis and $\mathbf{v}_{OH}$ is perpendicular to $\boldsymbol{\mu}_{H_2O_2}$ (x axis).

The OH product rotation is generated by the H–O–O bending vibraton and by the torsional mode in hydrogen peroxide, where the expectation value of $\langle J_z^2 \rangle \cong 450\,\mathrm{cm}^{-1}$ is generated by the bending modes of roughly planar H_2O_2 with the H atoms in *trans* position, while the origin of $\langle J_x^2 \rangle \cong 600\,\mathrm{cm}^{-1}$ is the internal torsional rotation of H_2O_2.

We have observed various correlations between the direction of recoil, the translational motion, the angular moment of fragments, and the transition dipole moment in the parent. Our aim was to show the successful feasibility of such measurements, since these correlations permit a direct insight into the final stage of the dissociation process. Further experiments are in progress in order to observe the dependence of the scalar and vectorial properties of the OH fragment, on the excess energy including the influence of the $\tilde{B}\,^1B$ state.

ACKNOWLEDGMENTS

This work has been performed as part of a program of the Deutsche Forschungsgemeinschaft. We thank Professor V. Staemmler (Bochum) for sending results of *ab initio* calculations on the H_2O_2 electronic states prior to publication and Professor E.-A. Reinsch (Frankfurt/M.) for helpful discussions.

[1] R. Bersohn, J. Phys. Chem. **88**, 5145 (1984).
[2] G. N. A. van Veen, K. A. Mohamed, T. Baller, and A. E. de Vries, Chem. Phys. **74**, 261 (1983).
[3] R. B. Bernstein, *Chemical Dynamics via Molecular Beam and Laser Technique* (Oxford University, New York, 1982).
[4] G. G. Balint-Kurti and M. Shapiro, Chem. Phys. **61**, 137 (1981).
[5] G. S. Ondrey, S. Kanfer, and R. Bersohn, J. Chem. Phys. **79**, 179 (1983); R. K. Sparks, K. Shobatake, L. R. Carlson, and Y. T. Lee, *ibid.* **75**, 3838 (1981).
[6] M. Shapiro and R. Bersohn, Annu. Rev. Phys. Chem. **33**, 409 (1982).
[7] E. J. Murphy, J. H. Brophy, and J. L. Kinsey, J. Chem. Phys. **74**, 331 (1981).
[8] P. Andresen, G. S. Ondrey, B. Titze, and E. W. Rothe, J. Chem. Phys. **80**, 2548 (1984); P. Andresen and E. W. Rothe, *ibid.* **78**, 989 (1983).
[9] R. Vasudev, R. N. Zare, and R. N. Dixon, J. Chem. Phys. **80**, 4863 (1984).
[10] I. Nadler, D. Mahgerefteh, H. Reisler, and C. Wittig, J. Chem. Phys. **82**, 3885 (1985); G. E. Hall, N. Sivakumar, and P. L. Houston, *ibid.* **84**, 2120 (1986).
[11] M. Dubs, U. Brühlmann, and J. R. Huber, J. Chem. Phys. **84**, 3106 (1986).
[12] R. Schmiedl, H. Dugan, W. Meier, and K. H. Welge, Z. Phys. A **304**, 137 (1982).
[13] G. E. Hall, N. Sivakumar, P. L. Houston, and I. Burak, Phys. Rev. Lett. **56**, 1671 (1986).
[14] G. Ondrey, N. van Veen, and R. Bersohn, J. Chem. Phys. **78**, 3732 (1983); A. Jacobs, K. Kleinermanns, H. Kuge, and J. Wolfrum, *ibid.* **79**, 3162 (1983).
[15] M. Suto and L. C. Lee, Chem. Phys. Lett. **98**, 152 (1983).
[16] H. Gölzenleuchter, K.-H. Gericke, F. J. Comes, and P. F. Linde, Chem. Phys. **89**, 93 (1984).
[17] C. B. McKendrick, E. A. Kerr, and J. P. T. Wilkinson, J. Phys. Chem. **88**, 3930 (1984).
[18] H. Gölzenleuchter, K.-H. Gericke, and F. J. Comes, Chem. Phys. Lett. **116**, 60 (1985).
[19] S. Klee, K.-H. Gericke, and F. J. Comes, J. Chem. Phys. **85**, 40 (1986).
[20] G. H. Dieke and H. M. Crosswhite, J. Quant. Radiat. Transfer **2**, 97 (1962).
[21] G. Herzberg, *Molecular Spectra and Molecular Structure, Spectra of Diatomic Molecules* (Van Nostrand, Princeton, 1950), Vol. 1.
[22] C. H. Greene and R. N. Zare, Annu. Rev. Phys. Chem. **33**, 119 (1982).
[23] T. Nagata, T. Kondow, K. Kuchitsu, G. W. Loge, and R. N. Zare, Mol. Phys. **50**, 49 (1983).
[24] G. M. Nathanson and G. M. McClelland, J. Chem. Phys. **81**, 629 (1984).
[25] C. H. Greene and R. N. Zare, J. Chem. Phys. **78**, 6741 (1983).
[26] U. Fano and J. H. Macek, Rev. Mod. Phys. **45**, 553 (1973).
[27] D. A. Case, G. M. McClelland, and D. R. Herschbach, Mol. Phys. **35**, 541 (1978).
[28] M. Nuss, K.-H. Gericke, and F. J. Comes, J. Quant. Spectrosc. Radiat. Transfer **27**, 191 (1982).
[29] W. L. Dimpfl and J. K. Kinsey, J. Quant. Spectrosc. Radiat. Transfer **21**, 233 (1979).
[30] S. R. Leone, Adv. Chem. Phys. **50**, 255 (1982).
[31] D. L. Baulch, R. A. Cox, R. F. Hampson, Jr., J. A. Kerr, J. Troe, and R. T. Watson, J. Phys. Chem. Ref. Data **9**, 295 (1980).
[32] C. Jonah, J. Chem. Phys. **55**, 1915 (1971); J. Solomon, C. Jonah, P. Chandra, and R. Bersohn, *ibid.* **55**, 1908 (1971).
[33] G. E. Bush and K. R. Wilson, J. Chem. Phys. **56**, 3638, 3655 (1972).

[34]S. Yang and R. Bersohn, J. Chem. Phys. **61**, 4400 (1974).
[35]J. L. Kinsey, J. Chem. Phys. **66**, 2560 (1977).
[36]J. P. Simons, J. Phys. Chem. **88**, 1287 (1984).
[37]R. N. Dixon, J. Chem. Phys. **85**, 1866 (1986).
[38]R. H. Hunt, R. A. Leacock, C. W. Peters, and K. T. Hecht, J. Chem. Phys. **42**, 1931 (1965); R. Block and L. Jansen, *ibid.* **82**, 3322 (1985).
[39]P. A. Giguere and T. K. K. Srinivasan found a value of 120° for the dihedral angle of the lowest energy state [P. A. Giguere and T. K. K. Srinivasan, J. Mol. Spectrosc. **66**, 168 (1977)].
[40]P. A. Giguere, J. Chem. Phys. **18**, 88 (1950); P. A. Giguere and O. Bain, J. Phys. Chem. **56**, 340 (1952); P. A. Giguere and K. B. Harvey, J. Mol. Spectrosc. **3**, 36 (1959).
[41]J. J. Lamb, Thesis, University of California, Irvine, 1982.
[42]V. Staemmler, Ruhr-Univ. Bochum (private communication).
[43]C. Chevaldonnet, H. Cardy, and A. Dargelos, Chem. Phys. **102**, 55 (1986).
[44]K. F. Freed and Y. B. Band, *Excited States*, edited by E. C. Lim (Academic, New York, 1977), Vol. 3, p. 109.
[45]A. D. Wilson and R. D. Levine, Mol. Phys. **27**, 1197 (1974).
[46]K. P. Huber and G. Herzberg, *Molecular Spectra and Molecular Structure, Constants of Diatomic Molecules* (Van Nostrand, Princeton, 1979), Vol. 4.
[47]R. Vasudev, R. N. Zare, and R. N. Dixon, Chem. Phys. Lett. **96**, 399 (1983).
[48]A. F. Tuck, Trans. Faraday Soc. **73**, 689 (1977).
[49]M. D. Morse and K. F. Freed, J. Chem. Phys. **78**, 6045 (1983); M. D. Morse, Y. B. Band, and K. F. Freed, *ibid.* **78**, 6066 (1983).
[50]H. Kijewski and J. Troe, Helv. Chim. Acta **55**, 205 (1972).
[51]P. Andresen and E. W. Rothe, J. Chem. Phys. **82**, 3634 (1985); R. Schinke, V. Engel, P. Andresen, D. Häusler, and G. G. Balint-Kurti, Phys. Rev. Lett. **55**, 1180 (1985).
[52]D. Cremer, J. Chem. Phys. **69**, 4440 (1978).
[53]R. Schinke, J. Phys. Chem. **90**, 1742 (1986).